8

A Comprehensive Performance Evaluation of a Short Duration High Speed Transient Flow Test Facility

Al-Falahi Amir[1], Yusoff M. Z[1], N. H. Shuaib[1] and Yusaf T[2]
(1) Universiti Tenaga Nasional UNITEN, College of Engineering, Jalan Kajang-Puchong, 43009 Kajang, Selangor Darul Ehsan, Malaysia
(2) University of Southern Queensland USQ, Faculty of Engineering and Surveying, Toowoomba 4350, Australia

Abstract
The aim of this article is to develop a numerical and experimental performance evaluation procedure to investigate the parameters affecting the flow conditions in a Short Duration High Speed Transient Flow Test Facility. For the numerical formulation, a two-dimensional time-accurate time-marching Navier-Stokes solver for shock wave applications was developed based on the dimensions of the test facility available at Universiti Tenaga Nasional (UNITEN) in Malaysia. The solver uses second-order accurate cell-vertex finite-volume spatial discretization and fourth order Runge-Kutta temporal integration scheme. The facility has been designed so that it can be used as a free piston compressor, shock tube, shock tunnel and gun tunnel interchangeably. It is expected that this facility will allow various researches to be done in the field of high speed (supersonic and hypersonic) fluid flows. The maximum Mach number obtainable depends on various operation conditions such as diaphragm pressure ratio, driver/driven gas combination and initial temperature ratio of the driver/driven gases. It was shown that a Mach number of 4 can be achieved if Helium is used as the driver gas and CO_2 is used as the driven gas with diaphragm pressure ratio of about 75. Two sets of experiments have been conducted; the first one using shock tube arrangement while in the second set the facility is used as a free piston compressor arrangement (shock tube with free piston). The experimental investigations involved pressure measurements using high precision pressure transducers and temperature measurements using an in-house made fast response thermocouple. The measurements yield the pressure and temperature histories, which were subsequently used to calculate the shock wave strength and the surface temperature change during the facility operation. In all cases, the analytical and experimental results were compared with the numerical results and good agreements were obtained. The results show that the facility performance in terms of shock speed, shock strength and the flow Mach number is highly affected by the diaphragm pressure ratio, gas combination and existence of piston.
Key words: shock tunnel, shock tube, shock wave, Computational Fluid Dynamics (CFD).

1. Introduction

In the study of high speed flow (supersonic and hypersonic) related to aerodynamics of aerospace vehicles, concepts such as heat transfer, non equilibrium flow, ionization, dissociation and other high temperature effects are very important. These effects are very difficult to model theoretically or computationally. It is also impossible to measure the flow conditions which are encountered by the aerospace vehicles during the actual flight; therefore high speed transient flow test facility is an important component in the design process of aeronautics equipment.

The problem of providing a source of air at a sufficiently high temperature and pressure, similar to those encounters by aerospace vehicle to act as the working fluid of wind tunnel has been approached in a variety of ways. Because of the high capital cost and also high operating cost associated with continuous high speed wind tunnels, most of the high speed flow test facilities, especially those of high temperature, are short duration blow down type. For example Hotshot tunnels, Plasma arc tunnels and light gas gun [1]. Furthermore, in high speed fluid flow problems, achieving a high Mach number is less important than achieving the correct flow enthalpy (temperature). This is because the high temperatures which developed around the stagnation region have a profound effect on the gas dynamics and aerodynamics [2]. Continuous facilities cannot provide high enthalpy flows due to design problems associated with heat transfer especially in nozzle and reservoir regions. Transient high speed flow test facilities are very attractive due to their ability to provide high enthalpy flows [3].

Short duration high speed transient flow test facility is a device that can be used to generate gas flows or gas conditions that are difficult to achieve in other test devices. By its nature, these facilities produce these conditions for a very short duration. The maximum achievable stagnation temperature or enthalpy in a short duration facility is an inverse function of flow duration. For example, expansion tubes can provide stagnation enthalpy in the order of 100 MJ/kg but only for tens of microseconds [4]. The useful flow duration in shock tunnels is longer (in the order of milliseconds) but the maximum stagnation enthalpy decreases to around 20 MJ/kg. Hotshot facilities that produce useful flows for around 100 ms have a maximum stagnation enthalpy of around 4 MJ/kg. Blow down tunnels are near continuous facilities that can provide long flow durations (measured in tens of minutes) but the maximum stagnation enthalpy is generally somewhat less than 4 MJ/kg [3].

In this article, a new short duration high speed transient flow test facility which has been developed in Universiti Tenaga Nasional – Malaysia is described. The test facility can be operated in four different modes, shock tube, free-piston compressor, shock tunnel and gun tunnel. All utilize the same basic facility and offer alternative modes of operation for the same apparatus. They differ in such away that, in shock tube and shock tunnel, the driver gas is employed to operate a shock tube containing the test gas, whilst in the free-piston compressor the free piston is used to directly compress the test gas in the driven section. The free piston in the gun tunnel compresses the test gas before ejecting it through a high speed flow nozzle.

The developed facility is the first of its kind in Malaysia. In other part of the world, there are currently existing facilities which can reach these high temperatures, but they are limited and rare. Free piston hypersonic shock tunnels have been constructed at California Institute of Technology (Caltech) in the United States and the German Aerospace Center (DLR Deutsches Zentrum fur Luft-und Raumfahrt) in Germany, but most of these high

temperature ground facilities were very costly to build and expensive to operate and maintain [5].
The main reason for development of the test facility is to enable aerodynamics study related to high speed flow. Apart from that, such high speed transient flow test facility is fundamentally important for the development of advanced instrumentation for high speed flow, for example, fiber optic pressure sensors and fast response thermocouples and investigation of flow and heat transfer in high speed low pressure turbine.
Although similar facilities have been built in a few parts of the world [5], there have been no open literatures available that describe the design procedures and important parameters that need to be considered when building such facilities. Hence, in the present work, a systematic approach has been developed in designing such facilities.
Historically, a large number of methods have been used to improve the performance of shock tubes and shock tunnels [6]. One method is to fill the driver section with a light gas such as helium. Another is to increase the temperature of the driver gas by use of a heater. In both of these methods, the improved performance is achieved by a higher speed of sound than if cold air is used. In the first case, the speed of sound in helium is higher than air because of its lower molecular weight. In the latter, the speed of sound is increased by raising the gas temperature. The higher sound speed results in a lower driver-to-driven tube pressure ratio P_4/P_1 required to generate a given incident shock Mach number in the driven tube, or a higher incident shock Mach number for the same value of diaphragm pressure ratio P_4/P_1.
Although both of the above mentioned approaches are well established, there are a number of disadvantages associated with them. Both require high pressure pumps and extensive plumbing. Helium is expensive and large amounts must be used to pressurize the driver tube. Helium's higher specific heat ratio also reduces the advantages somewhat. If the driver tube is to be heated, the tube must be designed to withstand high pressure under high temperatures, adding to the construction costs. The heater also adds to the cost and it must be designed to heat uniformly because hot spots in the driver can cause unpredictable and dangerous driver tube failure. Thermal fatigue may, in fact, limit the useful life of the tube.
For quite sometime, the free-piston driving technique, first proposed by Stalker [7], has been used to achieve some of the highest enthalpies, culminating in the X3 at the University of Queensland, Brisbane, Australia [8], the HEG in G¨ottingen, Germany [9] and the largest known facility, the HIEST in Kakuda, Japan [10]. The free-piston technique involves compressing the driver gas by a heavy piston accelerated to nearly sonic speed. The piston compresses the gas ahead of it to achieve high values of temperature and pressure. The operation of a free-piston shock tunnel, however, appears to be complicated, as a massive piston has to be accelerated rapidly and then must be stopped in a controlled manner.
Many methods of producing strong shock waves have been and are still being analyzed and tried experimentally.

2. Objectives and Methodology

The main objective of this study is to design and develop a short duration high speed transient flow test facility and investigate the parameters that influence the performance of the facility. The performance of this test facility is described by the maximum Mach number that can be generated and the quality of flows that it can produce. The Mach number

depends on the maximum temperature and pressure achievable. The facility is aimed to produce a targeted Mach number of 4.0. Different values of Mach number can be obtained by changing the diaphragm pressure ratio, different driver/driven gas combinations and by rising the driver gas temperature or in another word, increasing driver/driven gas temperature ratio T_4/T_1.

A theoretical model has been developed to determine the shock strength (P_2/P_1) and Mach number values as a function of diaphragm pressure ratio (P_4/P_1) and working fluids. Based on the theoretical model, the design procedure was developed. In order to verify the design, experimental measurements were performed which proved that the targeted Mach number can be achieved by using the prescribed pressure ratio and gas combinations determined by the design procedure.

In order to investigate the detail flow process inside the shock tube, which will influence its performance, a new two dimensional time accurate Navier-Stokes solver for shock tube applications was developed. The solver uses second order accurate cell-vertex finite volume spatial discretization and fourth order accurate Runge-Kutta temporal integration with Air-Air as working fluids. The solver is validated against experimental measurements in the developed high speed flow test facility. Further investigations were made on the flow process inside the shock tube by using the solver. The shock wave motion, reflection and interaction with the boundary layers were investigated and their influence on the performance of the shock tube was determined.

An in-house made surface junction fast response thermocouple was used to measure the surface temperature change profile during the facility operation. In order to evaluate the heat flux from the surface temperature change history, a MATLAB numerical transient heat transfer model was developed. Extensive experimental measurements were performed at different pressure ratios in order to investigate the performance of the facility. Pressure transient inside the tube were captured at two different locations using fast response transducers.

The last part of the work concerns with further experimental investigation of the performance of the facility using different gas combinations (dissimilar gases). The gas combinations used are He-Air and He-CO_2. The experimental results were compared with the theoretical predictions. The discrepancies were discussed based on the factors determined in the previous part.

3. Overview of UNITEN's Test Facility

There are three important limitations that govern the selection of the shock tube dimensions; cost, available space, and manufacturing process. Taking into consideration all these parameters, the decision was made to choose the dimensions of the test facility as described below. The detail components of the facility are described briefly and shown in Figure 1. More details about the facility are available in [11].

1. Driver section:- A high-pressure section (driver) which will contain the high pressure driver gas, which can be either Air, Helium, Hydrogen or other light gases.
2. Discharge valve:- To discharge the driver section after each run.

Pressure gauge:- To read the pressure inside the driver section, which is also provided with a static pressure transducer to record the exact value of the driver pressure P_4 at which the diaphragm ruptures.

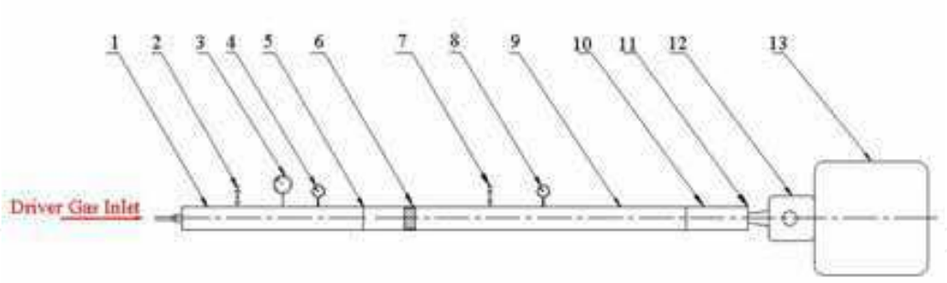

Fig. 1. Schematic of UNITEN's test facility

3. Vacuum pump:- When the driver gas is not Air (e.g. Helium or Hydrogen) then the driver section should be evacuated and refilled with the required driver gas.
4. The primary diaphragm:- This is a thin aluminum membrane to isolate the low-pressure test gas from the high-pressure driver gas until the compression process is initiated.
5. Piston compression section:- A piston is placed in the (driven tube) adjacent to the primary diaphragm so that when the diaphragm ruptures, the piston is propelled through the driven tube, compressing the gas ahead of it. This piston is used in the free-piston compressor and gun tunnel tests.
6. Discharge valve:- To discharge the driven section after each run.
7. Vacuum gauge:- To set the pressure inside the driven section to values less than atmospheric value (vacuum).
8. Driven section:- A shock tube section (smooth bore), to be filled with the required test gas (Air, nitrogen or carbon dioxide).
9. Driven section extension:- The last half meter of the driven section on which the pressure transducers and thermocouples are mounted.
10. The secondary diaphragm:- A light plastic diaphragm to separate the low pressure test gas inside the driven section from the test section and dump tank which are initially at a vacuum prior to the run.
11. Test section:- This section will expand the high temperature test gas through a nozzle to the correct high enthalpy conditions needed to simulate hypersonic flow. A range of Mach numbers is available by changing the diameter of the throat insert.
12. Vacuum vessel (dump tank):- To be evacuated to about 0.1 mm Hg pressure before running. Prior to a run, the driven section, test section and dump tank are to be evacuated to a low-pressure value.

4. Numerical Formulation of Flow Process

In this section, a two dimensional time accurate Navier-Stokes solver for shock tube applications is described briefly. The solver has been programmed based on the dimensions and configuration of the test facility. The developed solver uses second order accurate cell-vertex finite volume spatial discretization and fourth order accurate Runge-Kutta temporal integration and it is designed to simulate the flow process for similar driver/driven gases (e.g. Air-Air as working fluids). The solver is validated against analytical solution and experimental measurements in the high speed flow test facility. In the next section, further

investigations were made on the flow process inside the shock tube by using the solver. The shock wave motion, reflection and interaction with the boundary layers were investigated and their influence on the performance of the shock tube was determined.
It is intended that this CFD solver can be a useful tool in the design process of the test facility. Experimental data which could be achieved from the facility can be verified using this developed numerical tool.
The mathematical model and the fluid flow governing equations are described in ref [12]. This includes the Reynolds-Averaged Navier-Stokes Equations (RANS) and The Mixing Length Turbulence Model. The latter is added to the solver in order to include the viscous effects to the solution. Based on the facility dimensions, mesh generation procedure was performed to transform the flow domain into a finite number of grid points. Finally, using two verification approaches, the code was validated in terms of the ability to capture shocks, rarefaction waves and contact discontinuity and to produce the correct pressure, temperature, density and speed profiles, using two verification approaches. The first one was the validation against a standard analytical solution of the shock tube problem. The second was to compare the code solution with selected experimental measurements for a certain value of diaphragm pressure ratio. Further details about the solver can be found in [12].

5. Selected Case Studies

In this section, in order to obtain greater understanding of the processes involved, CFD simulations were used for selected cases and the results were analyzed in details. In order to investigate the effect of various parameters on the performance of the facility, various experimental measurements were made. The parameters that were investigated were pressure ratio, gas combination and effect of piston. This section provides detail discussions of the results obtained.

5.1 Inviscid Transient Flow in Shock Tube

CFD solution for an inviscid simulation of a diaphragm pressure ratio P_4/P_1 of 10 has been chosen for a detail investigation. The simulation was conducted using the actual dimensions of the test facility shown in Figure 1. The pressure, temperature, density and Mach number of the flow were stored in two stations at the end of the driven section with an axial separation of 342 mm, as shown in Figure 2.

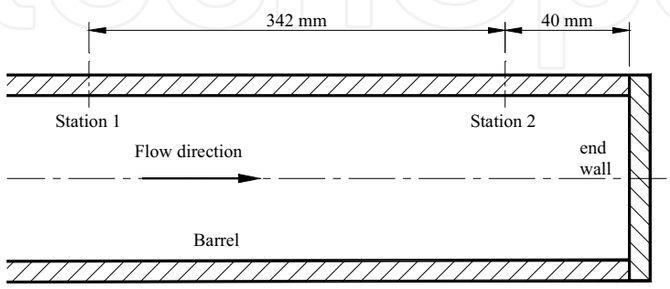

Fig. 2. The two stations at the end of the facility

The pressure history for the above mentioned shot is depicted in Figure 3 from which one can follow the physics of the flow inside the shock tube. The first jump represents the shock wave, for which the pressure inside the driven section increases from 100 kPa to around 220 kPa. As the shock wave proceeds to the end of the tube it will reflect and move in the opposite direction, increasing the pressure to about 450 kPa. The shock wave will then interact with the contact surface which is following the shock wave and due to this interaction between the shock wave and the contact surface the pressure will be increased until it reaches its peak pressure value of 530 kPa.

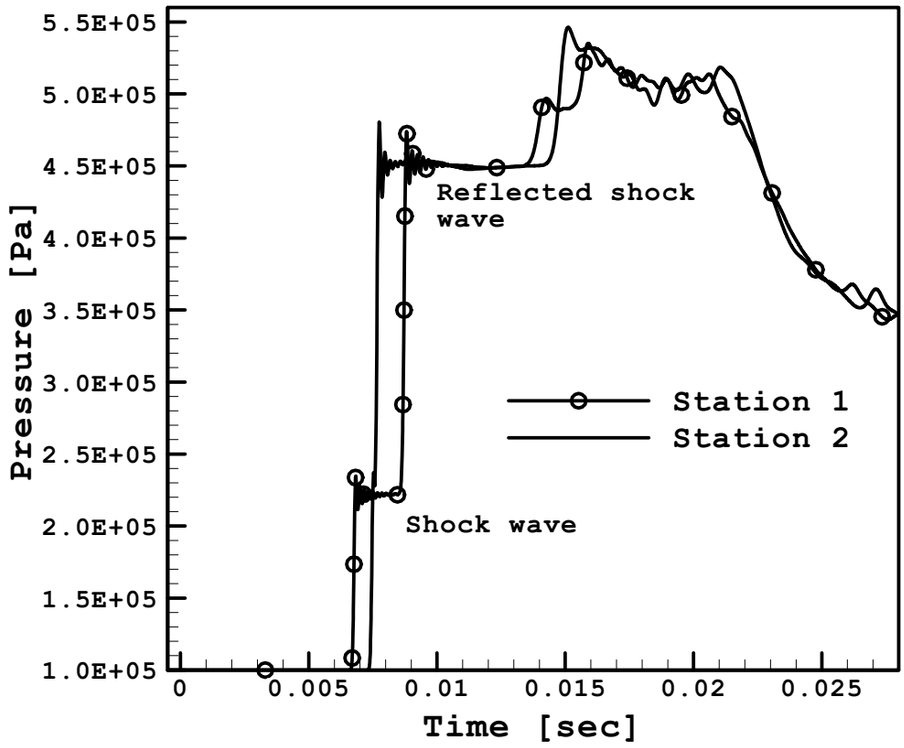

Fig. 3. Pressure history for inviscid flow (Air-Air, P_4/P_1=10)

The shock wave speed can be determined from the CFD data obtained in this simulation. As the distance between the two stations is known (0.342 m) and the time of the shock to travel from station 1 to station 2 can be obtained from the pressure history graph (see Figure 4), the shock wave speed in this case was calculated to be 518 m/s. Comparing this value to the theoretical value for this pressure ratio, which is 558 m/s, the percentage difference was found to be around 7%. The difference is probably due to the two-dimensional effects which were not modeled by the theoretical solution. From experimental measurements the shock speed for the same pressure ratio was 450 m/s, which indicate percentage difference of about 13% from CFD results.

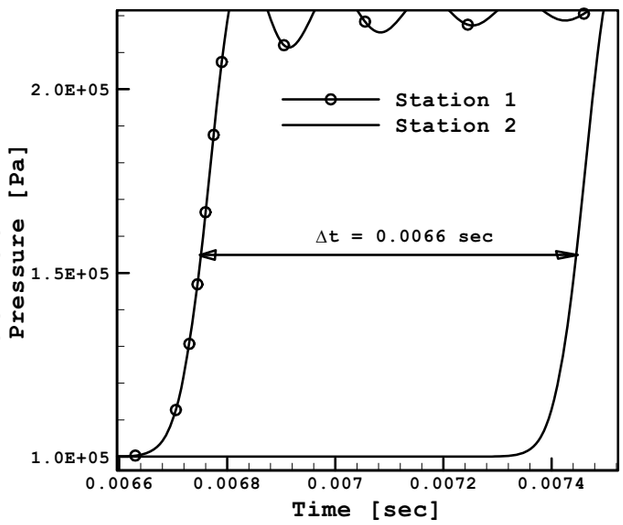

Fig. 4. Shock wave speed (inviscid flow)

Using the same procedure, the reflected shock wave speed can be determined. As the wave reflects from the tube end and moves in the opposite direction (left direction), due to impact with the end wall the wave will lose some of its kinetic energy due to the collision with the end wall and consequently its speed decreases to about 342 m/s.
The same trend can be noted when the temperature history is investigated, as shown in Figure 5. The first jump in the temperature profile represents the shock wave and the second jump is due to the reflected shock wave. The temperature is increased from the initial value 300 K to about 380 K due to shock wave effect. When the shock reflects from the tube end, the temperature rises to 475 K and after interaction between reflected shock wave and the contact surface, the flow temperature becomes about 490 K.

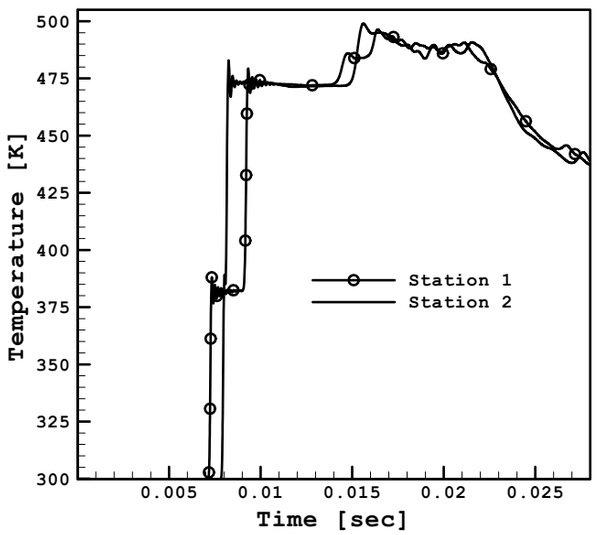

Fig. 5. Temperature history inside the shock tube (inviscid flow)

In order to have an overall view of what is happening inside the tube after diaphragm rupture, the *x-t* diagram for both pressure and density are depicted in Figures 6 and 7 respectively. From these two figures, the inviscid flow process inside the tube can be fully described. After diaphragm ruptures a shock wave travels along the driven section followed by a contact surface compressing the test gas inside the driven section causing high pressure and temperature. At the same time a rarefaction waves travels in the opposite direction along the driver section, decreasing the driver pressure and temperature. Both shock and expansion waves will be reflected after getting to the end of the tube and the shock wave interacts with the contact surface.

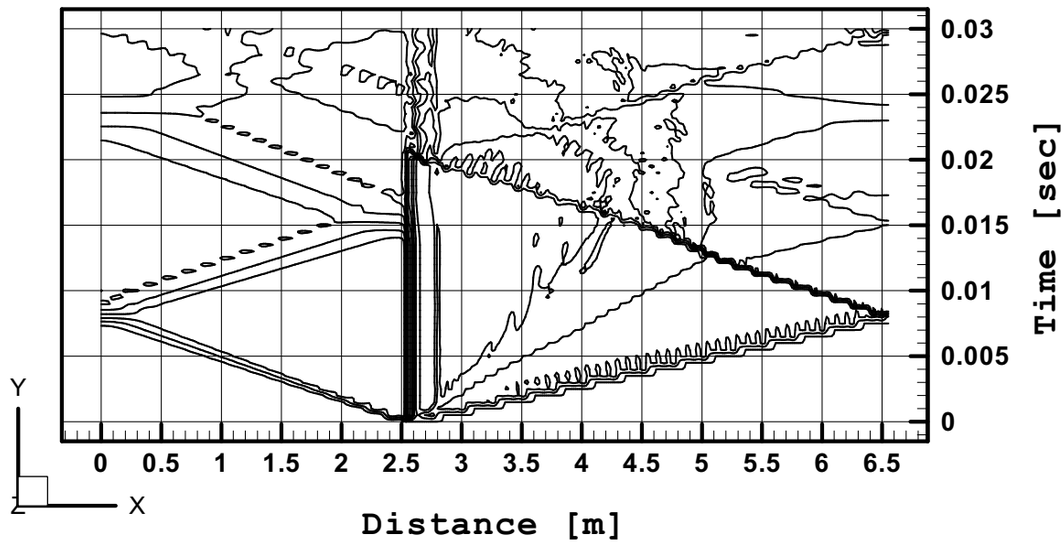

Fig. 6. *x-t* diagram for pressure profile (inviscid flow)

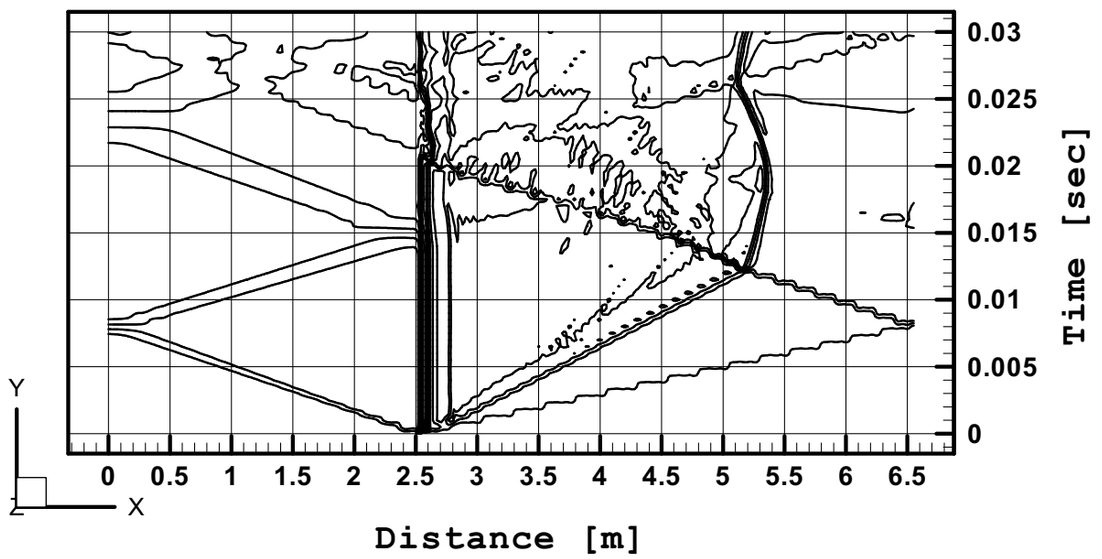

Fig. 7. *x-t* diagram for density profile (inviscid flow)

It is interesting to note that after interaction with the reflected shock wave, the contact surface remains at about the same position, indicating achievement of the tailored condition. The presence of the bush is also seen to have prevented the rarefaction wave and the shock wave from passing to the other section. The rarefaction wave and the shock wave are reflected when they reach the bush.
The contour plots of the pressure along the facility are shown in Figures 8 to 13. At time t = 0, the driver pressure P_4=100 kPa and pressure in the driven section P_1 is 10 kPa.

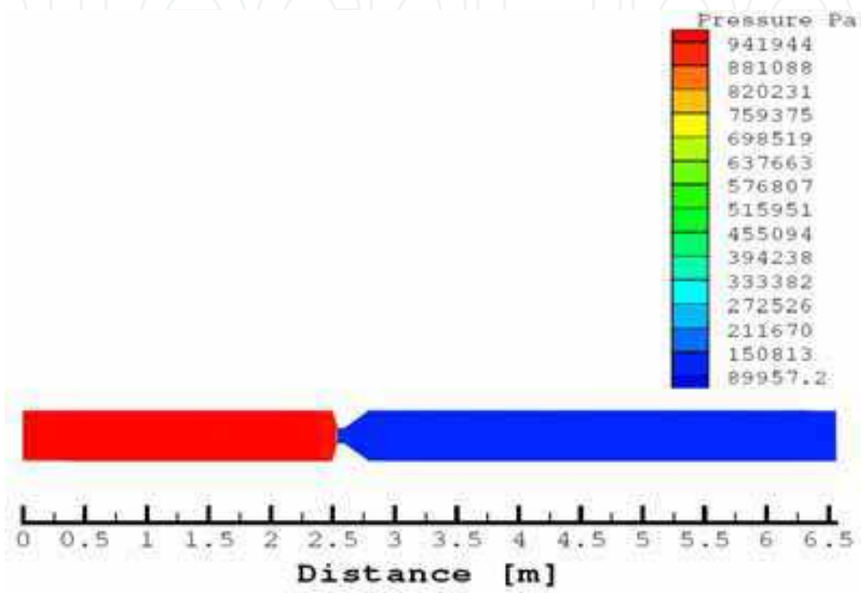

Fig. 8. Contour plot for pressure history at t = 0

After diaphragm rupture, shock wave travels to the right through the driven section while the expansion wave travels to the left through the driver section. These two waves are captured after 0.005 sec and shown in Figure 9.

Fig. 9. Shock and expansion waves at t = 0.005 sec

The two waves continue their journey towards the tube ends, at time 0.0078 s the shock wave hits the driven section end on the right hand side while the expansion wave reaches the left hand side of the facility as shown in Figure 10.

Fig. 10. Shock and expansion waves at the facility ends t = 0.0078 sec

At time t = 0.0082 sec, both waves reflect from the end of the tube as shown in Figure 11.

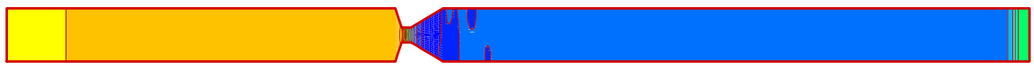

Fig. 11. Shock and Expansion waves' reflection at t = 0.0082 sec

The reflected shock wave now moves to the left towards the contact surface while the reflected expansion wave moves to the right towards the bush section as shown in Figure 12.

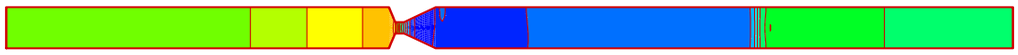

Fig. 12. Reflected waves move towards the contact surface at t = 0.0134 sec

The shock wave interacts with the contact surface and reflects again. This process continues until pressure balance along the whole facility as shown in Figure 13.

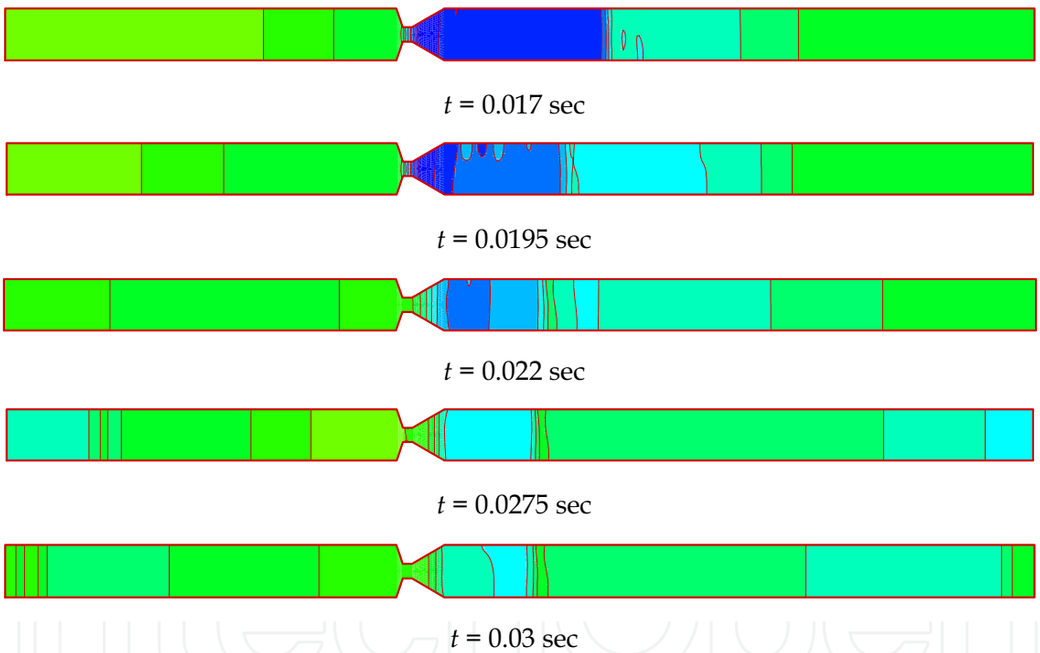

Fig. 13. Interaction between shock wave and contact surface

5.1.1 Two-Dimensional Effects

The presence of the bush has caused the flow in the facility to be two-dimensional and this requires two-dimensional CFD simulations. The contour plots of the velocity in x-direction along the facility at selected times are shown in Figure 14. As the shock wave reflects from the tube end it will move to the left and interact with the contact surface and the flow is no longer symmetry as shown in Figure 15.

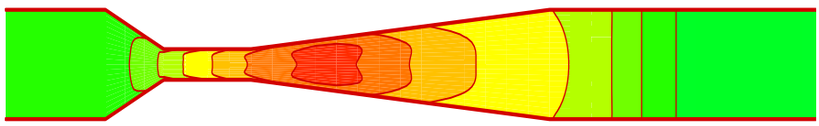

a: Velocity contour before shock reflection (t = 0.0007 sec)

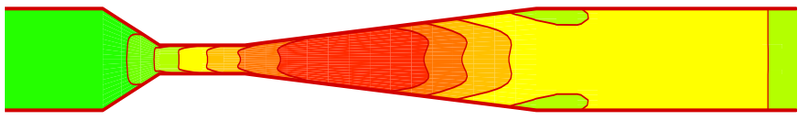

b: Velocity contour before shock reflection (t = 0.001 sec)

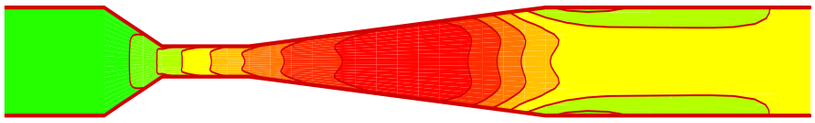

c: Velocity contour before shock reflection (t = 0.0015 sec)

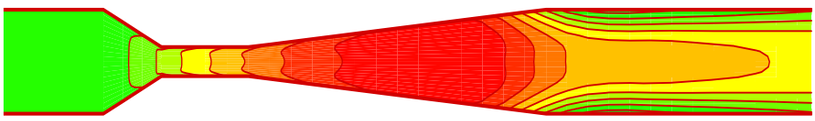

d: Velocity contour before shock reflection (t = 0.003 sec)

Fig. 14. Velocity contour plots in x-direction at selected times

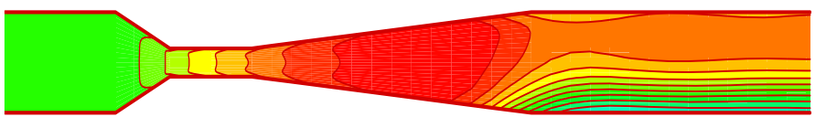

Fig. 15. Velocity contour after shock reflection and interaction with contact surface (t = 0.0125 sec)

The velocity contours at t = 0.02 sec after diaphragm rupture are shown in Figure 16. It can be observed that the flow is highly two-dimensional especially in the region close to the bush in the driven section. It is interesting to note that after t = 0.0125 sec, the velocity in area close to the bush becomes asymmetric. The asymmetry becomes more and more obvious as time progress and creates a recirculating region, which extend to about 10 times the bush inner diameter along the x-axis.

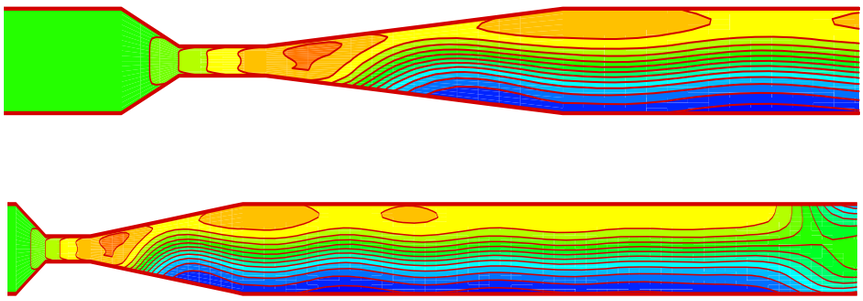

Fig. 16. Velocity contour after shock reflection and interaction with contact surface (t = 0.02 sec)

To investigate further, the velocity profiles at different times at x = 279 mm from the diaphragm section are plotted in Figures 17 to 19. As shown in the figures, at time t = 0.001 sec the profile is perfectly symmetrical. However, the velocity profile contains inflexion part, which according to Drazin and Reid [13] is unstable and susceptible to disturbances. The asymmetry becomes more apparent as the process continues. The upper half of the tube has mainly positive velocity whereas the bottom half has negative velocity.

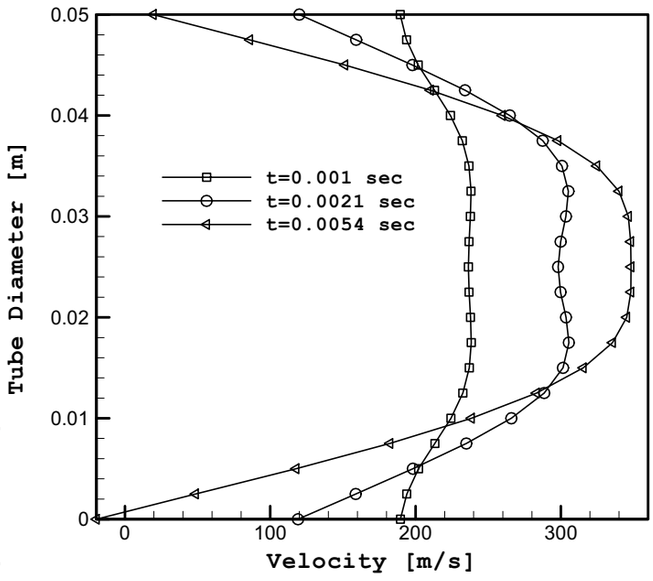

Fig. 17. Velocity section profile after diaphragm rupture at x = 279 mm from diaphragm

The formation of the recirculating region in this inviscid simulation is surprising especially considering that the tube is symmetrical [14]. However, it has been previously reported by Xu Fu et al. [15] that high speed flow tends to become unstable when shock wave interacts with contact discontinuity.

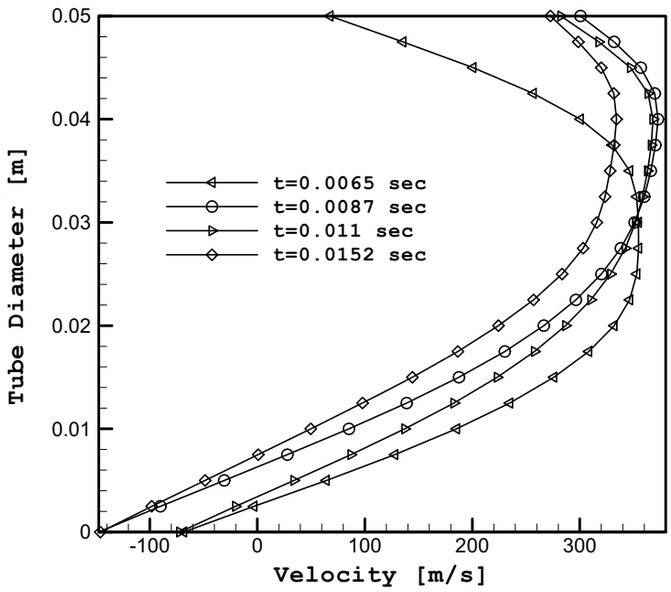

Fig. 18. Velocity profile after shock reflection at x = 279 mm from diaphragm section

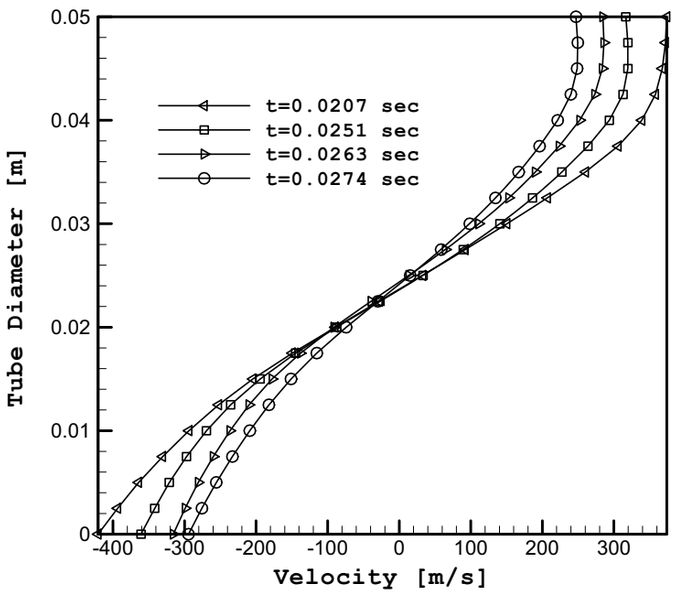

Fig. 19. Velocity profile after shock interaction with contact surface at x = 279 mm from diaphragm section

In order to get deeper understanding to what is happening inside the shock tube after diaphragm rupture; velocity, pressure, temperature and density profiles below tube axis (25% of the tube diameter), along the tube axis (50% of the tube diameter) and above tube axis (75% of the tube diameter) were depicted at different times. Figure 20 shows the results at t = 0.005 sec. At this time, the fluid velocity immediately jumps from zero to 500 m/s

which is greater than speed of sound in air, consequently a shock wave is generated and starts to move to the right. The profiles at 25%, 50% and 75% of the tube diameter follow the same trend whereby pressure decreases from 1000 kPa to 800 kPa, the temperature increases from 300 to 400 K and the density drops from 11.5 kg/m^3 to 9.8 kg/m^3. Similar to the velocity profile, the pressure, temperature and density profiles at 25%, 50% and 75% of the tube diameter along the facility follow the same trend.

It can be noted that there is a sudden change in the pressure, temperature and density curves in the diaphragm region. This is due to cross sectional area change where the diameter decreases from 50 mm to 30 mm which is the bush diameter. The bush is located adjacent to the thin aluminum diaphragm and it is used to facilitate the rupture process.

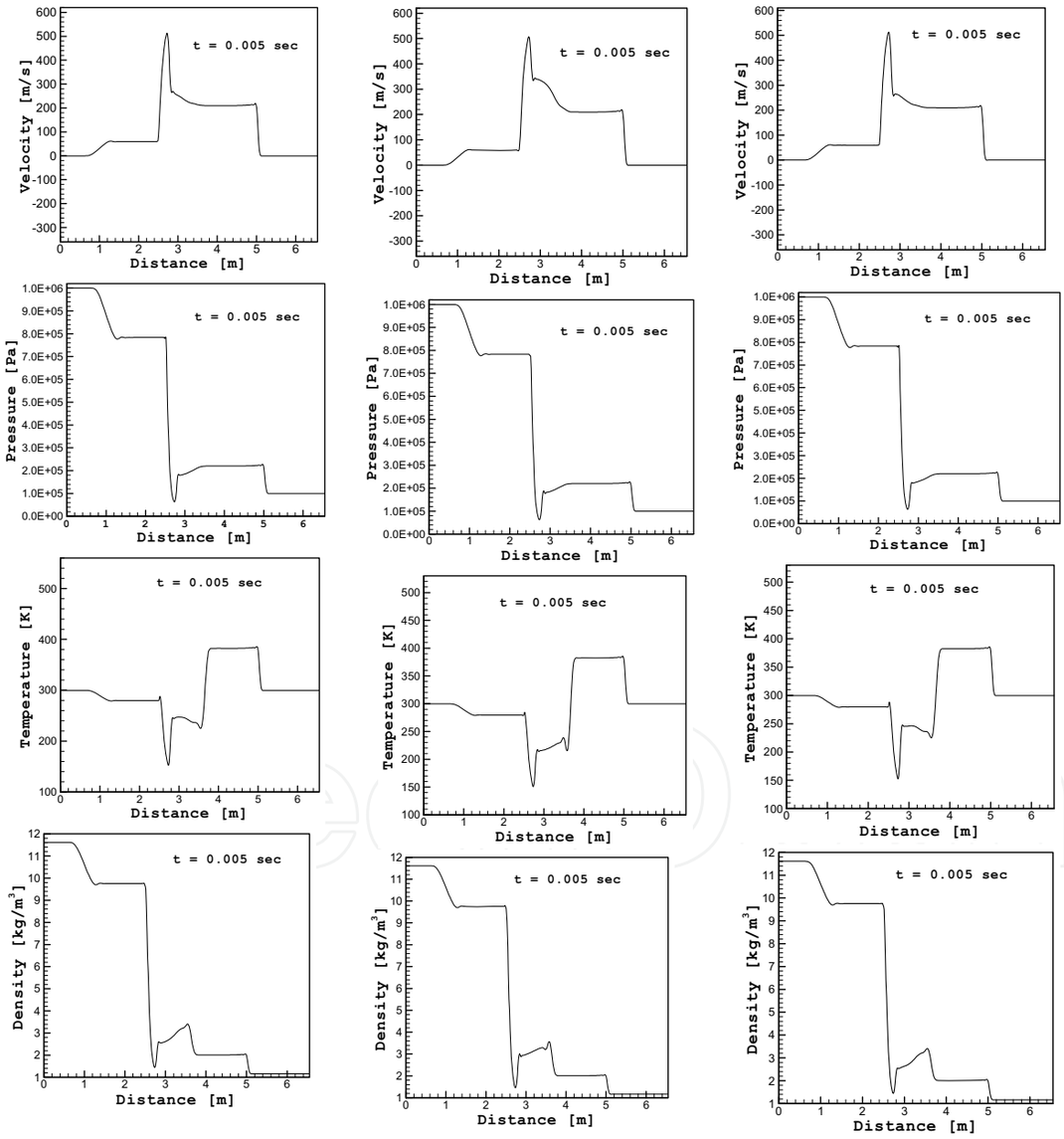

a: 75% b: 50% c: 25%

Fig. 20. Velocity, Pressure, Temperature and Density profiles at t = 0.005 sec

Figure 21 shows the flow profiles after shock reflection. From the velocity profiles at this time, it can be seen that the flow is still symmetry about the tube longitudinal axis, however, it can be noted that asymmetry has already started. Pressure, temperature and density along the driven section (except the bush section) are all increased due to the effect of the compression waves.

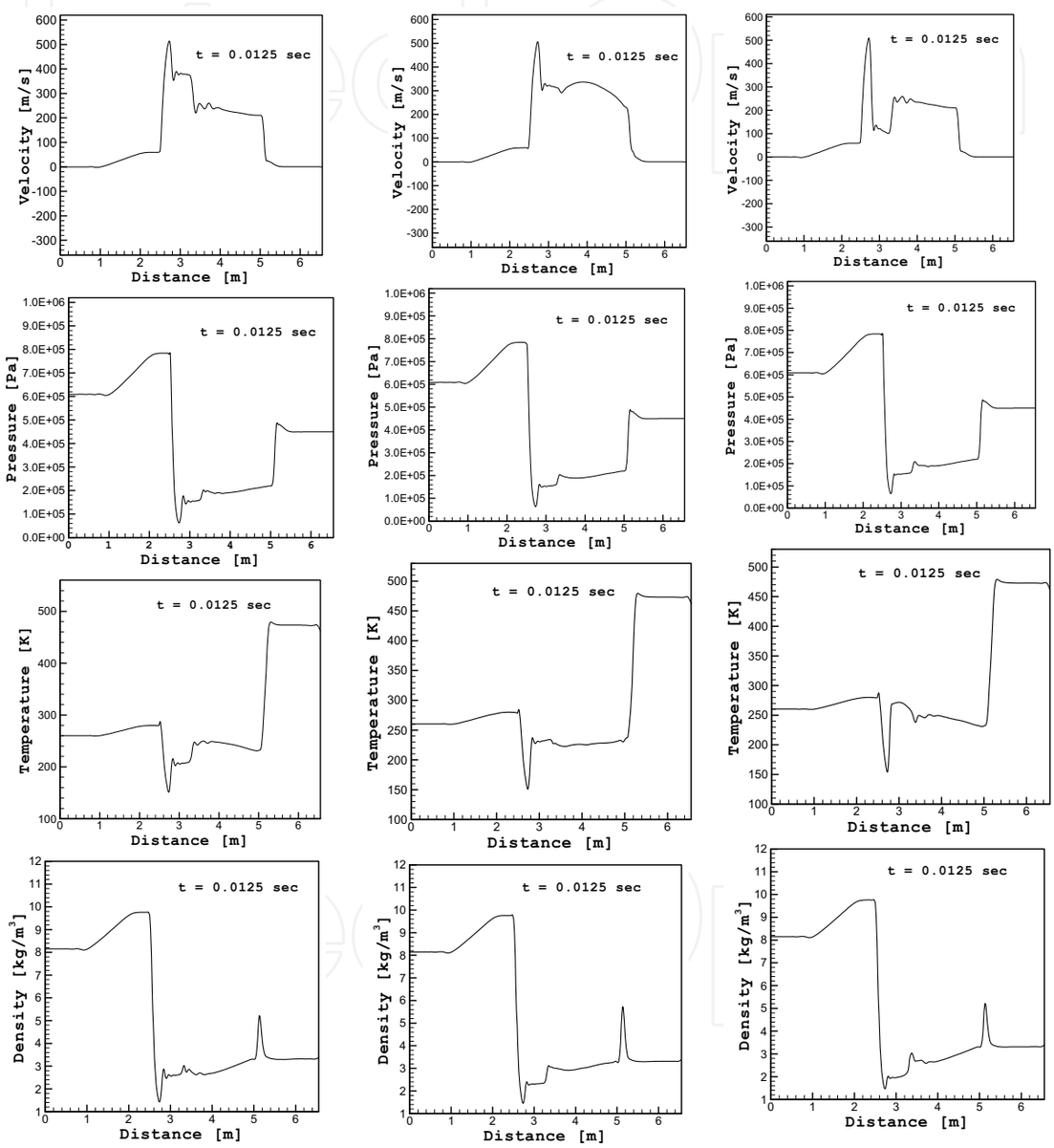

a: 75% b: 50% c: 25%

Fig. 21. Velocity, Pressure, Temperature and Density profiles at t = 0.0125 sec

At t = 0.175 sec, the flow non-uniformity becomes clearer as shown in Figure 22.

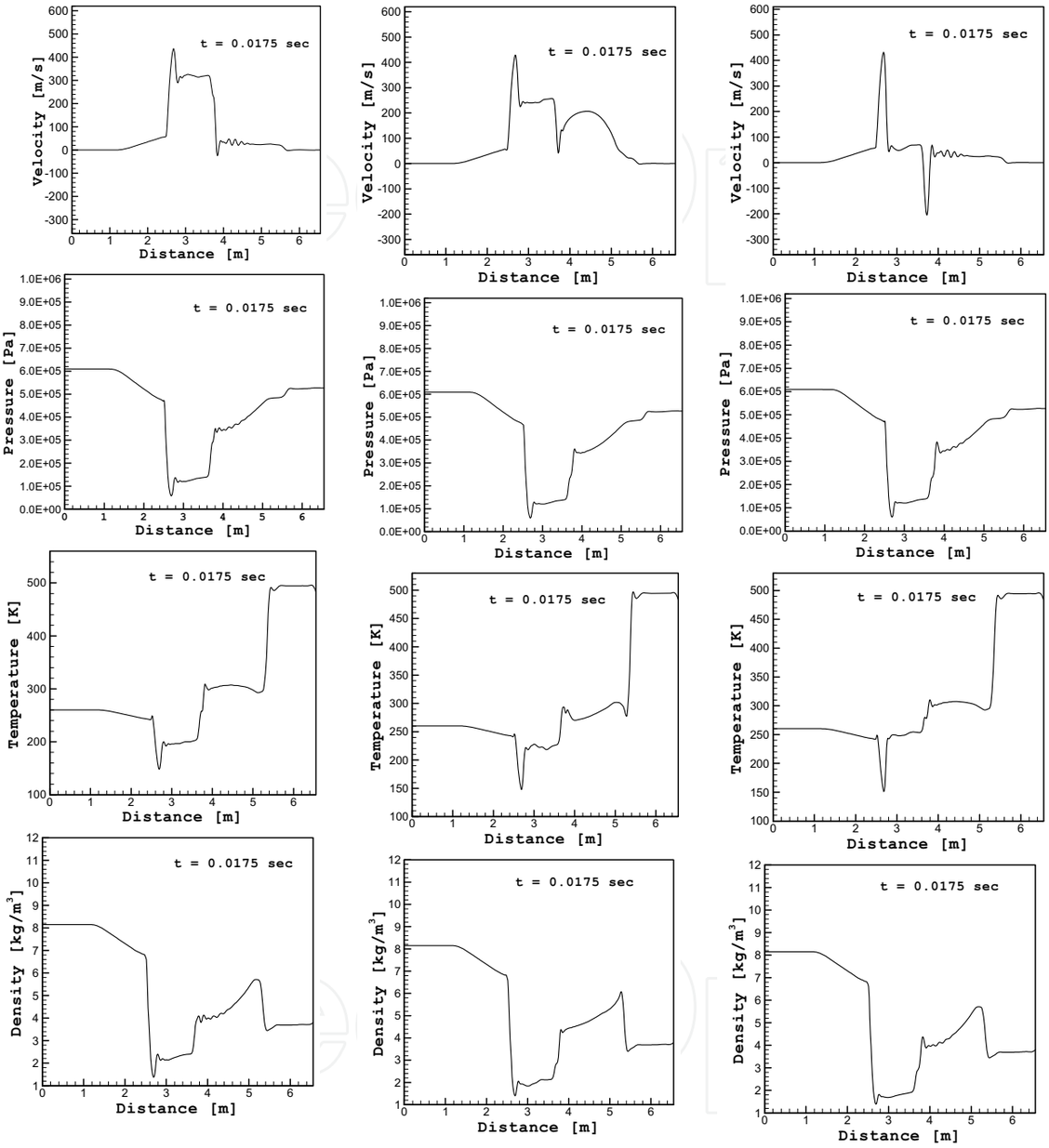

a: 75% b: 50% c: 25%

Fig. 22. Velocity, Pressure, Temperature and Density profiles at t = 0.0175 sec

As the reflected shock proceeds to the left, asymmetric flow becomes very clear as shown in Figure 23. The gas flows to the right in the upper side while it flows to the left in the bottom side of the tube, as can be seen from velocity profile shown in Figures 24.

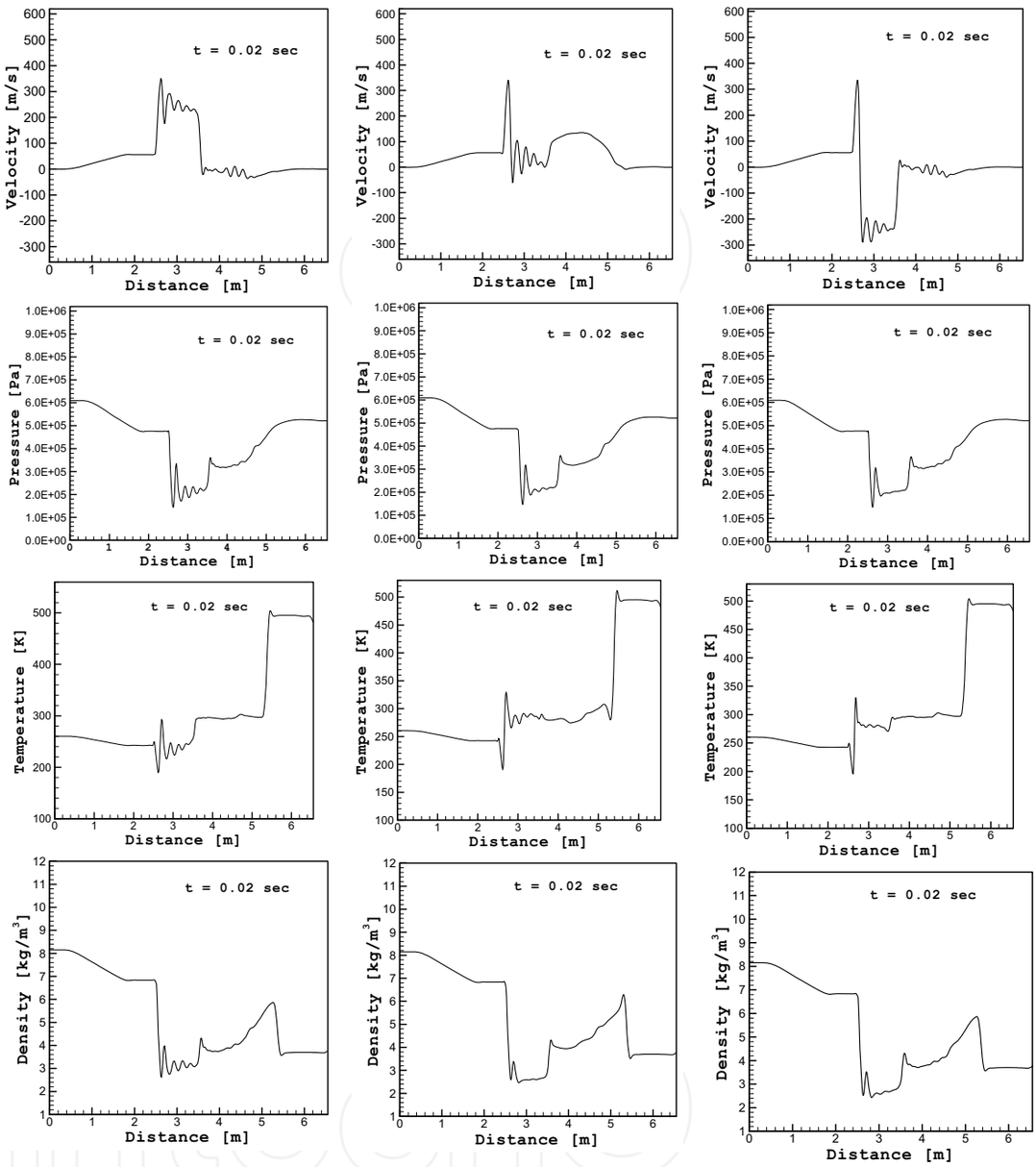

a: 75% b: 50% c: 25%

Fig. 23. Velocity, Pressure, Temperature and Density profiles at t = 0.02 sec

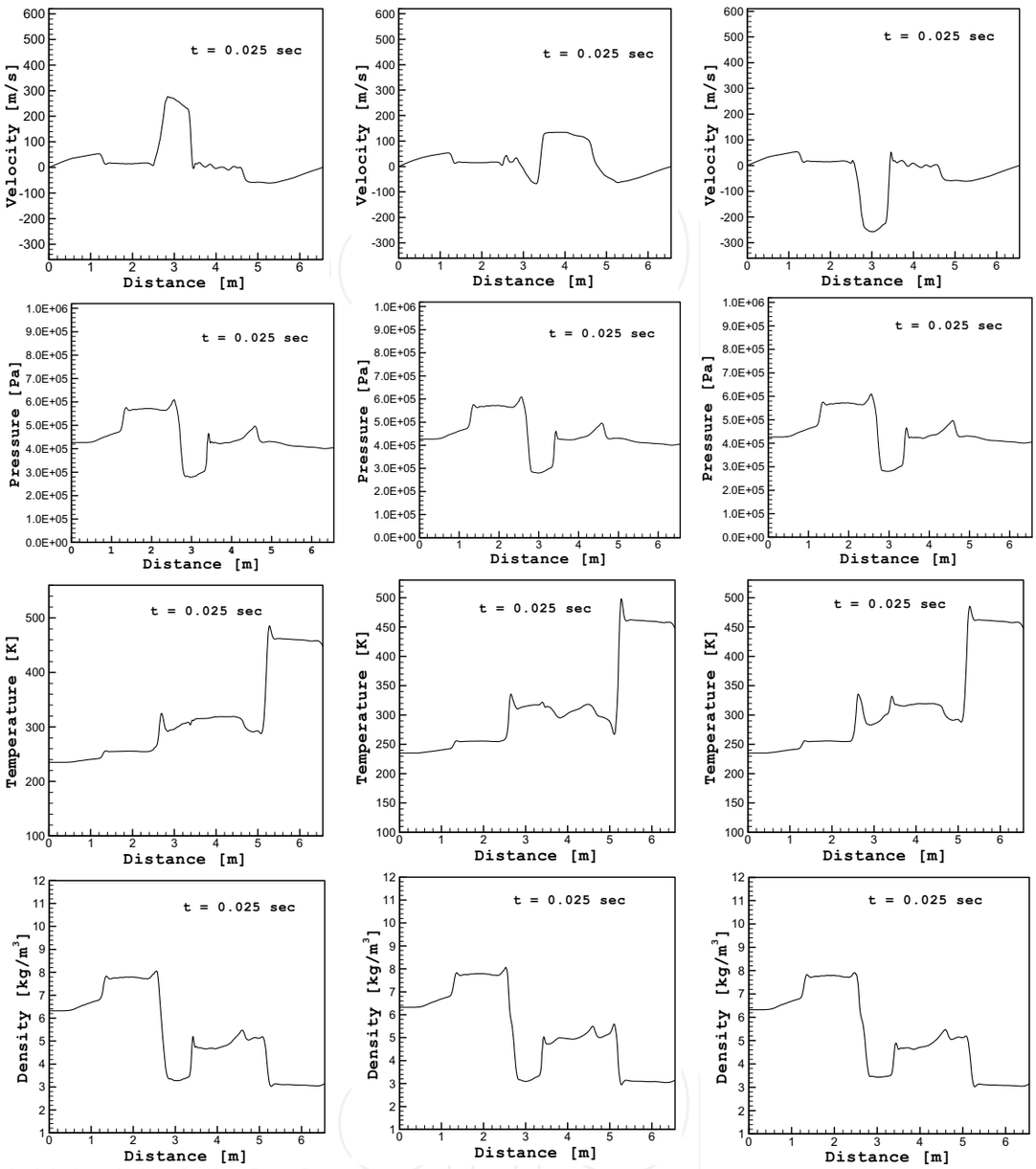

a: 75% b: 50% c: 25%

Fig. 24. Velocity, Pressure, Temperature and Density profiles at t = 0.025 sec

After a series of frequent reflections the gas becomes more quiescent and moves towards a balance state as shown in Figure 25.

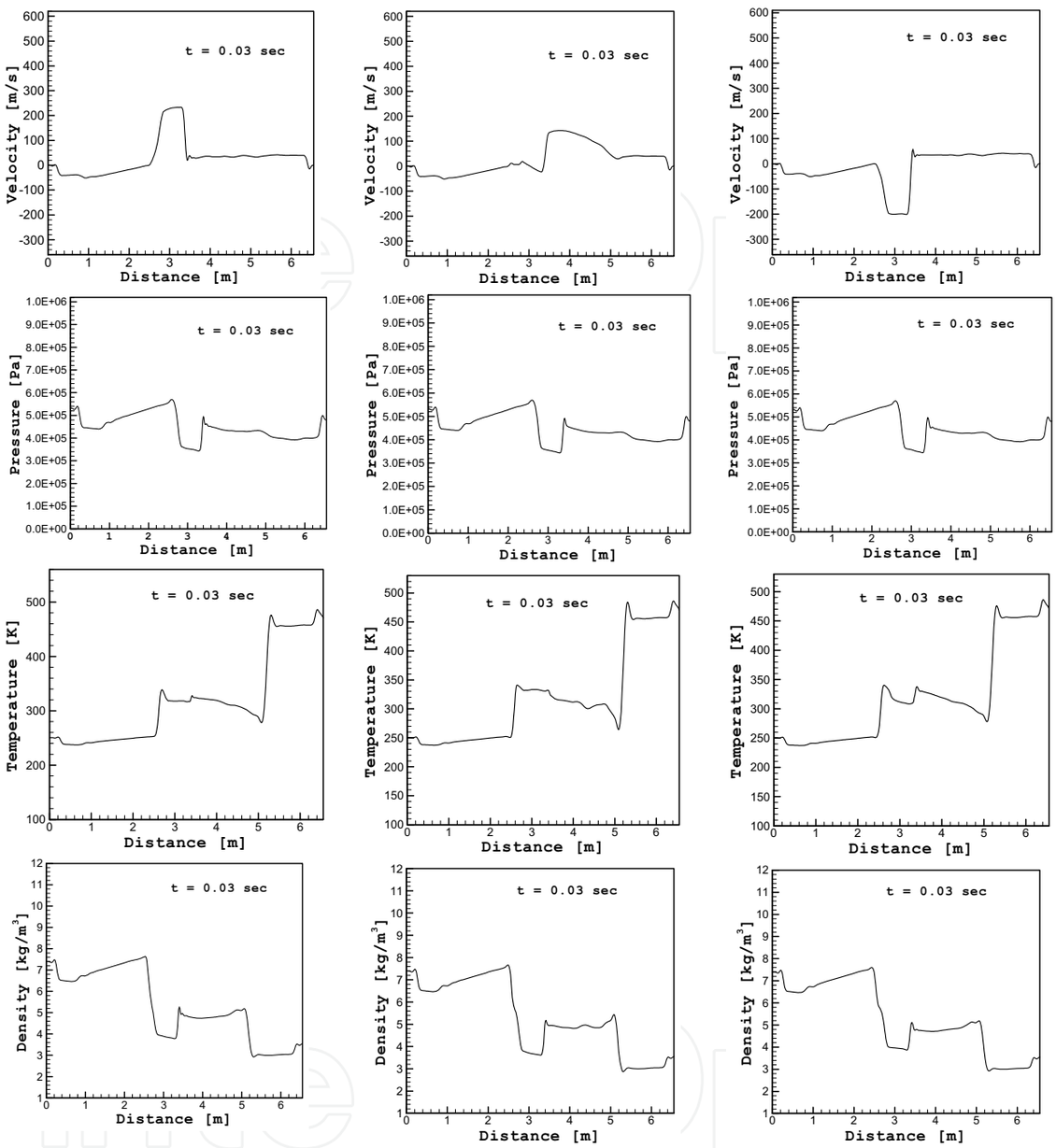

a: 75% b: 50% c: 25%

Fig. 25. Velocity, Pressure, Temperature and Density profiles at t = 0.03 sec

5.2 Viscous Transient Flow in Shock Tube

In order to investigate the effect of viscosity on the transient flow in shock tube and how it affects the performance of the facility, a viscous simulation has been conducted using the same boundary conditions as for the inviscid simulation presented in the previous section. The pressure history for the above mentioned shot is depicted in Figure 26. The Figure shows similar trend as for the inviscid flow. The first jump represents the pressure rise due

to shock wave, for which the pressure inside the driven section increases from 100 kPa to around 220 kPa. The shock wave then reflects as it hits the end of the tube and moves in the opposite direction, subsequently rising the pressure to about 450 kPa.

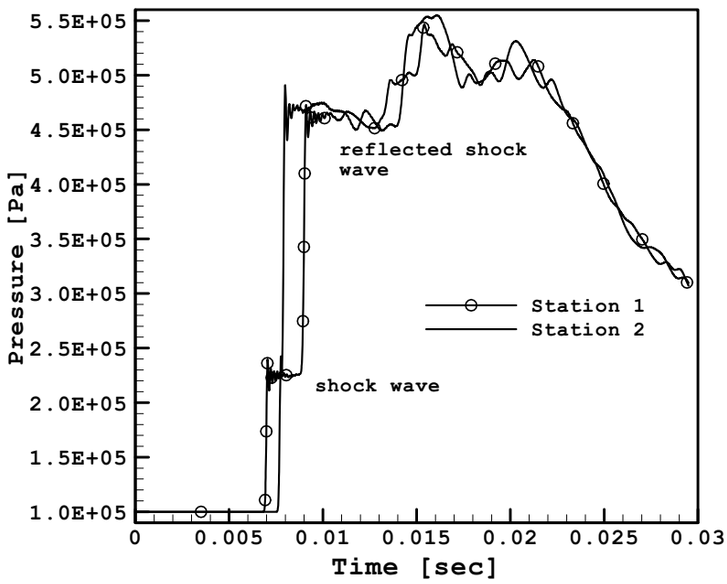

Fig. 26. Pressure history for viscous flow (Air-Air, P_4/P_1=10)

The shock wave will then interact with the contact surface (which is following the shock wave) and due to their interaction, the pressure will be increased until it reaches its peak pressure value, which is equal to around 530 kPa in this case.
Using similar procedure as outlined previously, the shock wave speed in this case was calculated to be 456. Comparing to the inviscid value for the same pressure ratio obtained previously (518 m/s) the effect of viscosity becomes obvious. It can be deduced that viscosity decreases the shock wave speed to about 11% due to the boundary layer effects. From experimental measurements the shock speed for the same pressure ratio was 450 m/s, which indicated percentage difference of about 1.3% from the CFD result.

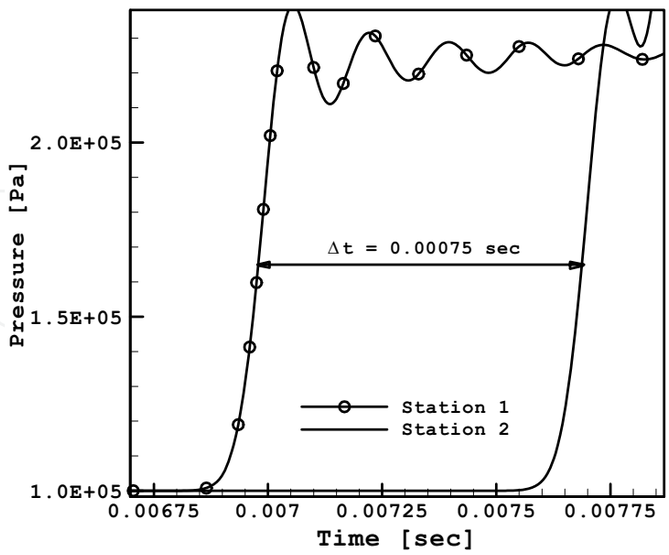

Fig. 27. Shock wave speed (viscous flow)

After it hits the tube end, shock wave will be reflected and moves to the left with a slower wave speed of about 311 m/s. Comparing with respect to the reflected shock wave speed for inviscid flow which is 342 m/s, it is apparent that viscosity resists the fluid motion causing slower speed of the shock wave by 9.1%.
Analyzing the temperature history for this simulation, it can be seen that the trend is quite similar to pressure history. The temperature results for this run have been displayed in Figure 28. The first jump represents the shock wave and the second jump is due to the reflected shock wave. The temperature is increased from the initial value of 300 K to about 500 K.

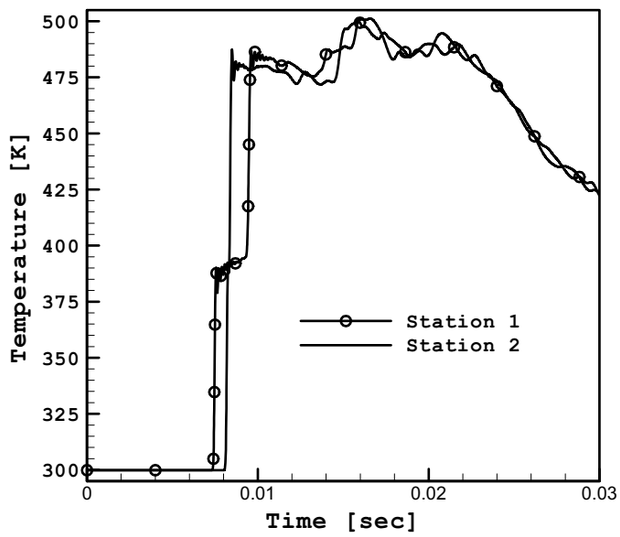

Fig. 28. Temperature history inside the shock tube (viscous flow)

Figure 29 and 30 show *x-t* diagram for pressure and density profiles respectively. It can be noted from Figure 30 that the intersection point between the reflected shock wave and the contact surface occurred at 5.35 m as compared to inviscid flow at 5.15 m (as shown in Figure 7); this indicates slower shock speed for the viscous flow and hence confirm the above calculation of shock speed.

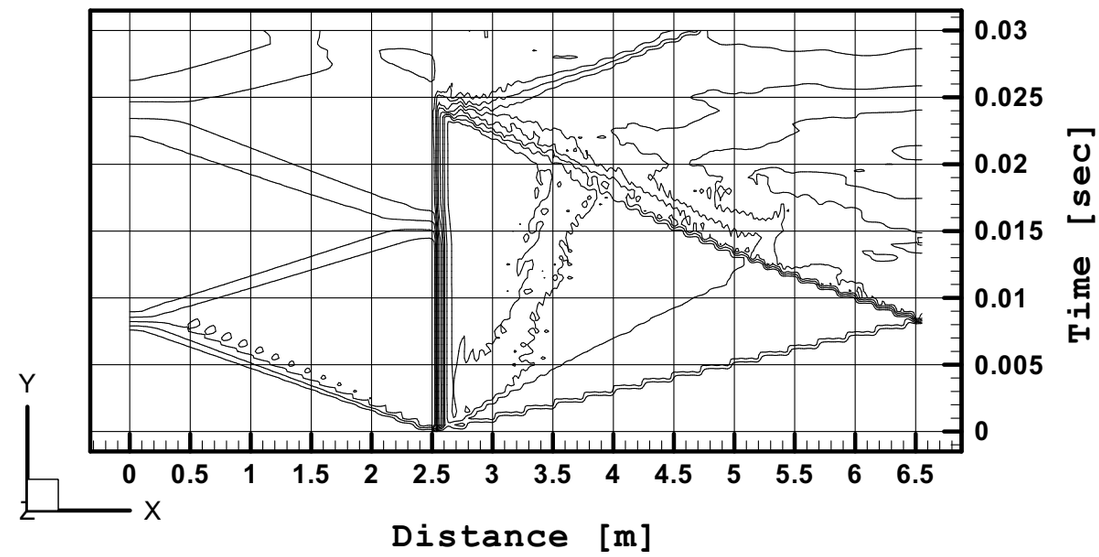

Fig. 29. *x-t* diagram for pressure profile (viscous flow)

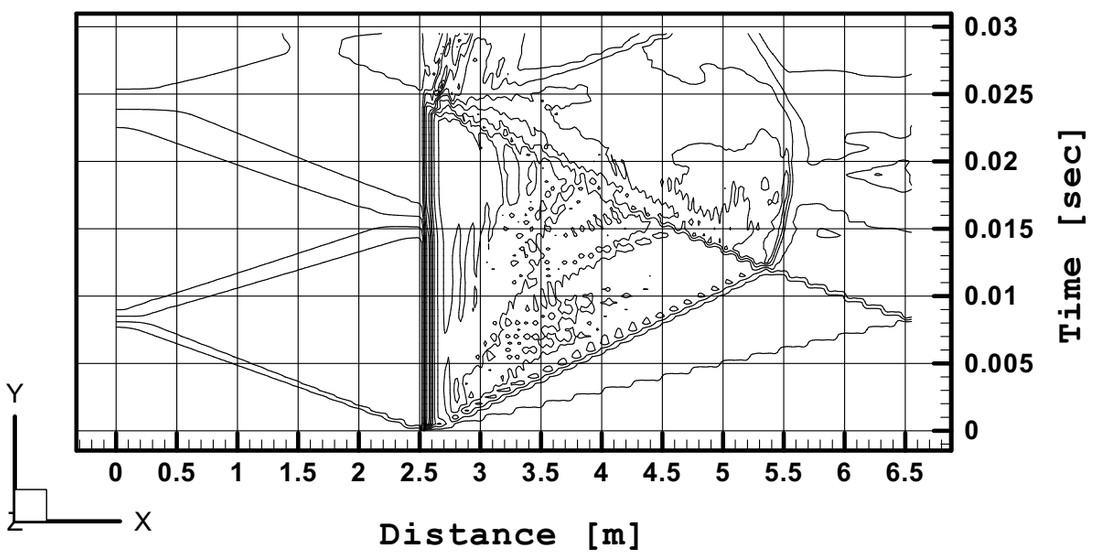

Fig. 30. *x-t* diagram for density profile (viscous flow)

Figure 30 shows the so-called tailored interface, where no disturbance is reflected from the contact surface back towards the rear wall of the shock tube. The "tailored" contact surface

configuration offers a number of advantages when applied to the operations of shock tubes, it increases the testing-time and it improves the homogeneity of the working gas parameters (i.e. it decreases possible contamination effects in the test section caused by the driver gas). As shown in Figure 30, the maximum useful duration time that can be obtained when the prescribed pressure ratio P_4/P_1 =10 is about 10 ms, which is quite comparable to other facilities.

5.2.1 Shock Wave - Boundary Layer Interaction

Ideally, the reflection of a shock wave from the closed end of a shock tube provides, for laboratory study, a quantity of stationary gas at extremely high temperature. Because of the action of viscosity, however, the flow in the real case is not one-dimensional and a boundary layer grows in the fluid following the initial shock wave. In the flow following the initial shock wave, there is a boundary layer generated near the walls of the shock tube, across which the velocity of the flow decreases from that in the main stream to zero at the walls.
Figure 31 shows the velocity profiles at x = 279 mm from the diaphragm after shock wave passes through it. It can be seen that the boundary layer thickness grows rapidly causing more blockage to the flow. It can be seen from Figure 31 that the shock wave speed remains constant as it moves towards the end of the tube. The shock wave speed reduces after reflection but it remains constant until it interacts with the contact surface. After that, there is evidence showing that the shock wave is attenuated and speed reduces. This is due to the effect of the boundary layer on the shock wave which cause additional blockage to the motion. The attenuation of shock wave due to interaction with boundary layer has been reported by McKenzie [15].

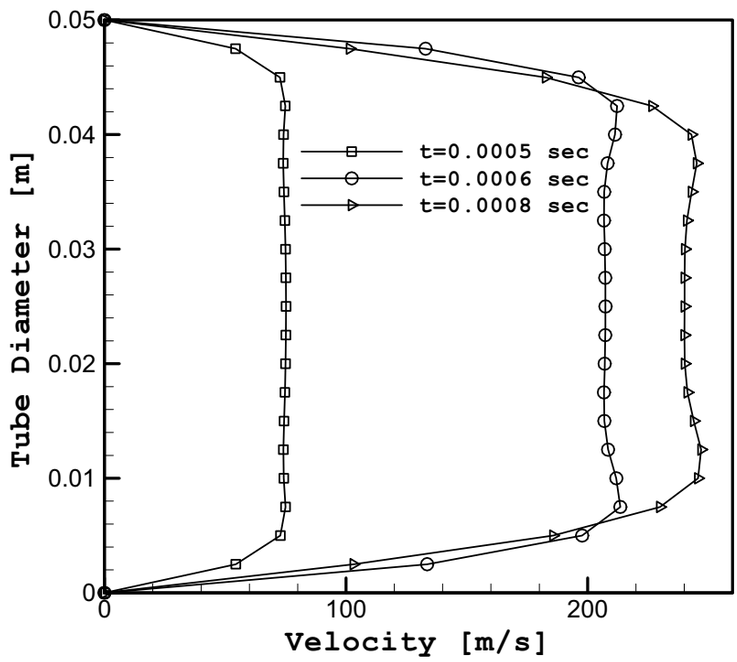

Fig. 31. Velocity profile after diaphragm rupture (viscous flow) at x = 279 mm from the diaphragm section

In section 5.1.1, it has been shown that the inviscid flow tend to be very unstable in the region close to the bush after shock wave interacts with contact surface and the recirculating flow has developed. In order to investigate the effect of viscosity to this performance, Figure 32 to 34 shows the evolution of the velocity profiles for viscous flow case. It can be seen in Figure 34 that before the shock wave was reflected, after 0.0005 sec from diaphragm rupture, the boundary layer separation has occurred close to the tube wall and the separated region grows.

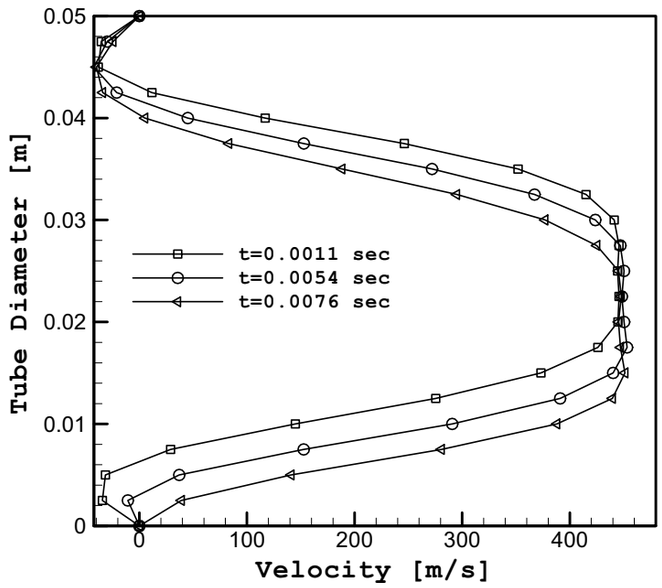

Fig. 32. Velocity profile at different times (viscous flow) at x = 279 mm from the diaphragm section

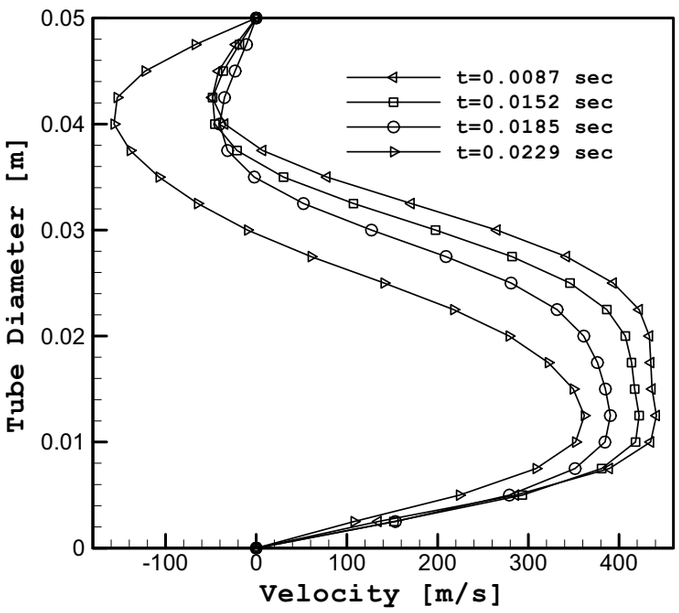

Fig. 33. Flow after shock reflection at x = 279 mm from the diaphragm section

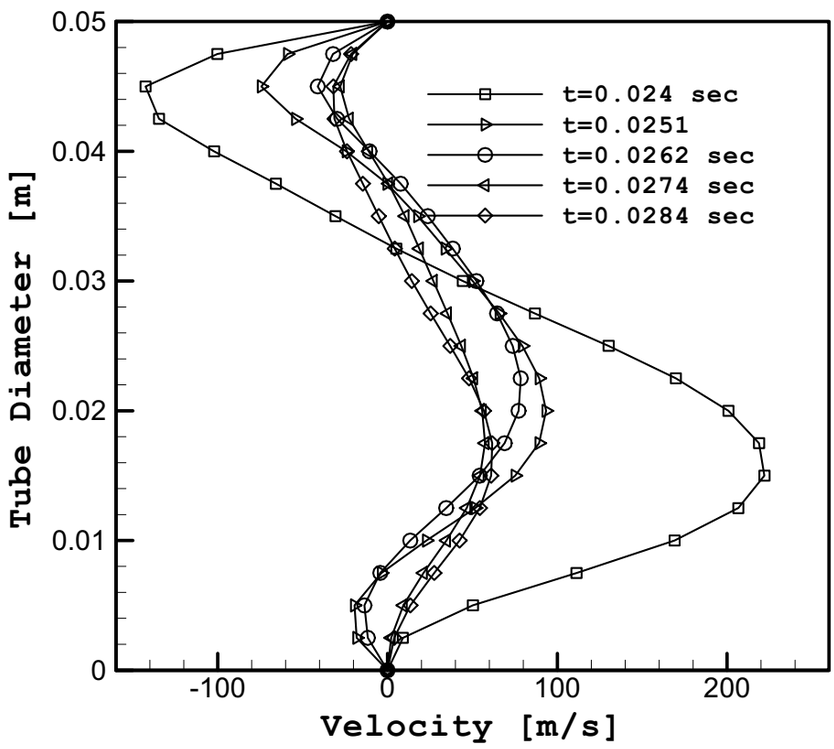

Fig. 34. Velocity profile after waves interaction at x = 279 mm from the diaphragm section

After the shock wave reflection and subsequent interaction with the contact surface, the separated flow region evolves into a full re-circulating region rotating in the anticlockwise direction. Then the flow returns back to the small separated flow region close to the tube walls.

5.3 The Effect of Diaphragm Pressure Ratio on the Facility Performance

It has been reported by many researchers that increase in diaphragm pressure ratio, P_4/P_1 will increase the peak pressure, temperature and shock wave speed. In the current work, experimental measurements have been performed for various pressure ratios varying from 8 to 55. CFD simulations were also performed for selected cases. Figures 35 and 36 show the measured pressure for P_4/P_1 8.8, 15 and 20 at station (1) and station (2 respectively. For comparisons, the CFD results are also plotted. It can be observed that the agreement between measurement and CFD are remarkably good.

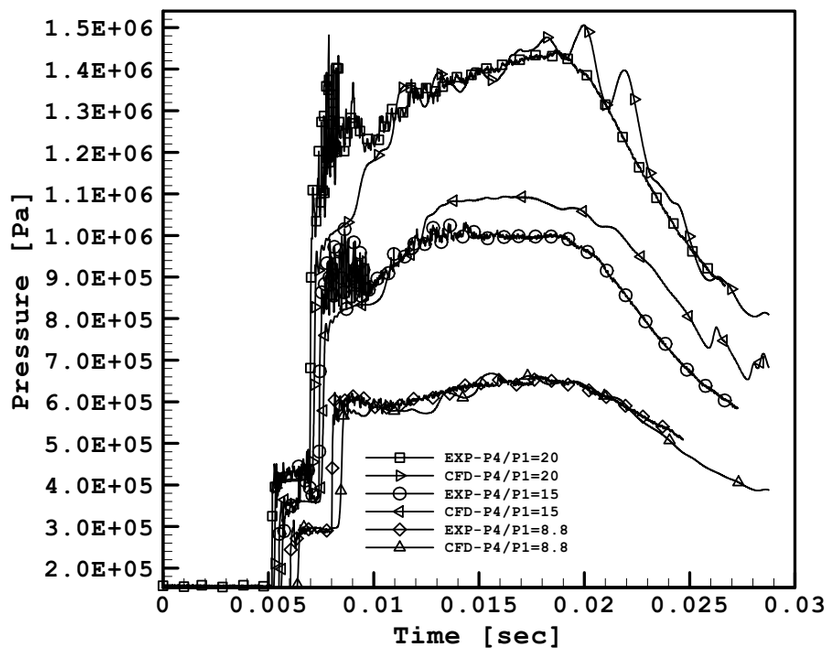

Fig. 35. Pressure history at station (1) for different pressure ratios (Air-Air)

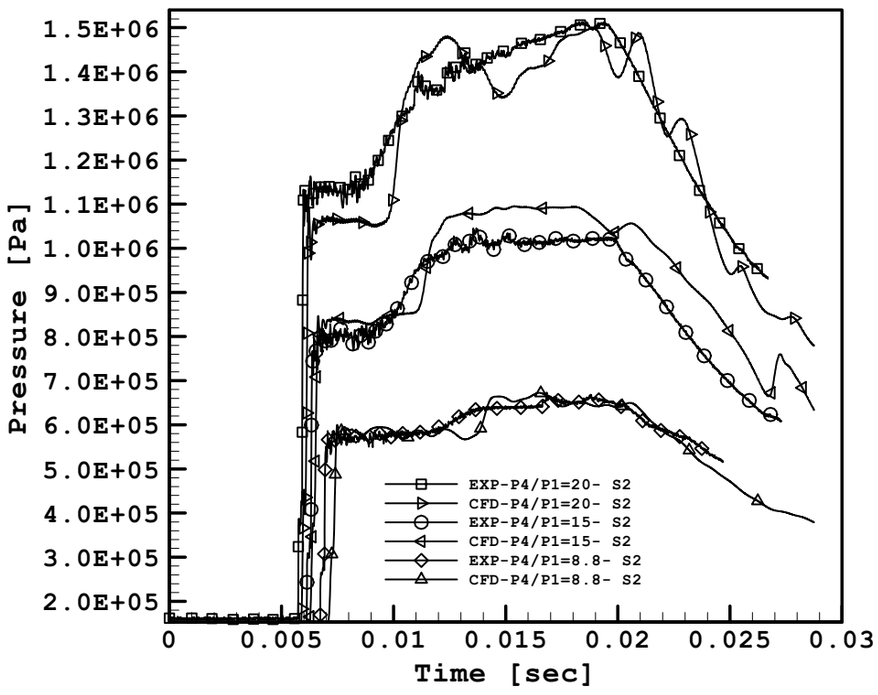

Fig. 36. Pressure history at station (2) for different pressure ratios (Air-Air)

Figures 35 and 36 show that as the pressure ratio increases, the pressure rise and the shock speed increases. The recorded initial rises are 280 kPa, 320 kPa and 420 kPa for pressure ratio 8.8, 15 and 20 respectively. After the shock reflection, the pressure rise further to 580 kPa, 800 kPa and 1000 kPa for pressure ratio 8.8, 15 and 20 respectively.
The corresponding temperature histories are shown in Figure 37. It can be seen that the temperature rise to 500 K, 575 K and 625 after the shock reflection for pressure ratios 8, 15 and 20 respectively. This clearly indicates that the pressure ratio has the effect of rising the temperature and hence the enthalpy of the gas.

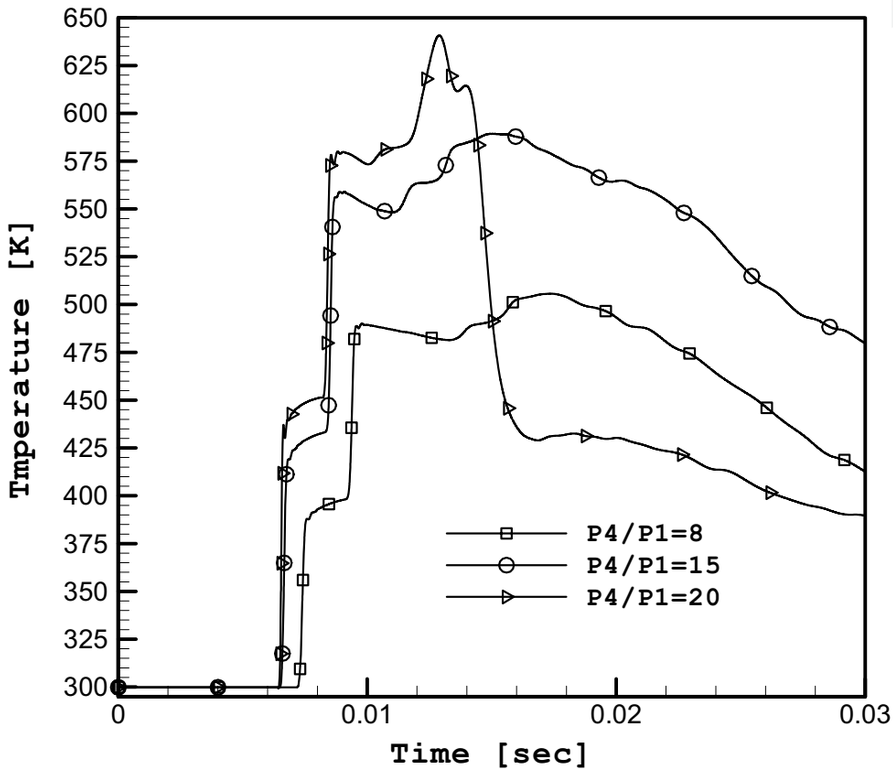

Fig. 37. Temperature history for different pressure ratios (Air-Air)

The measured shock strength (P_2/P_1) at different pressure ratios are plotted in Figure 38. Also plotted on the same graph are the theoretical and CFD predictions. It can be seen that, in generally, the measured pressure rise is about 16% lower than the theoretical values and closer to CFD predictions. This is due to the two-dimensional effect and viscous effects which are not modeled by the theoretical solution. However, the trend is very similar. As anticipated, the shock strength increases with increase in the pressure ratio. As pressure ratio is increased, the rate of increase of the shock strength decreases.

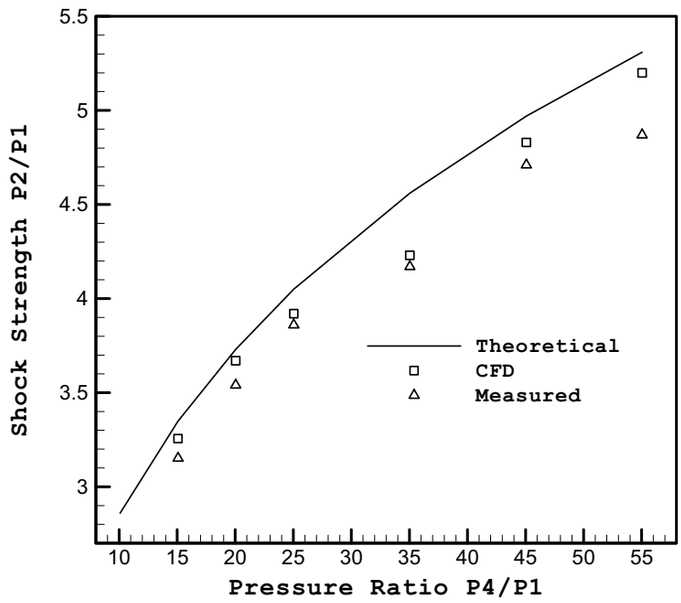

Fig. 38. Shock strength P_2/P_1 vs. diaphragm pressure ratio P_4/P_1

Figures 39 and 40 show the measured, theoretical and CFD results for shock speed and shock Mach number respectively. The Mach number is calculated based on the speed of sound of the undisturbed gas. The measured and CFD data are generally lower than the theoretical data and the agreement between CFD and measured data is very good. For the highest allowable pressure ratio of 55, the maximum shock Mach number is 2.116 when Air was allocated in both the driver and driven sections.

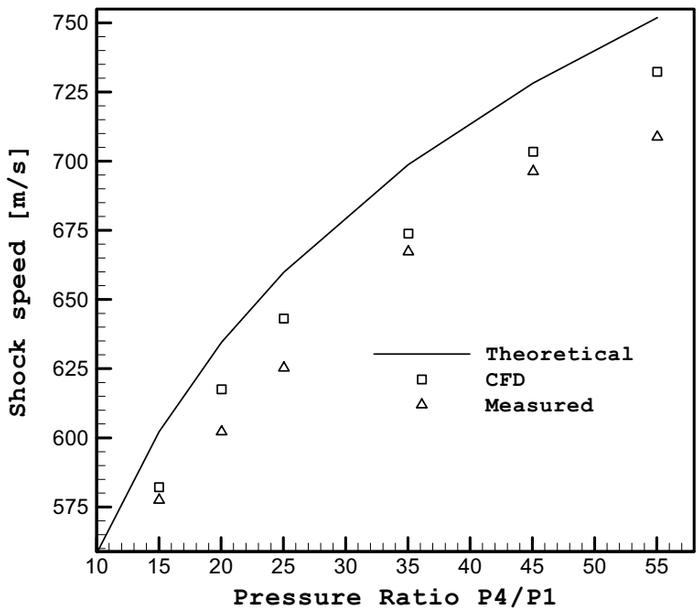

Fig. 39. Shock speed vs. diaphragm pressure ratio P_4/P_1

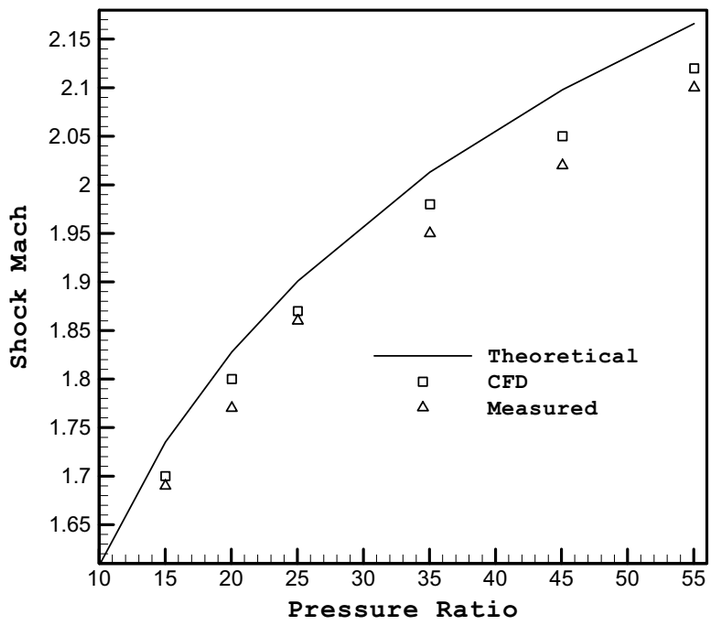

Fig. 40. Shock Mach number vs. diaphragm pressure ratio P_4/P_1

Figure 41 shows the measured peak pressure variation with pressure ratio. The peak pressure is defined as the maximum pressure achieved after shock reflection and subsequent interaction with contact surface, which further increases the pressure. It can be seen that the peak pressure rise increase when the pressure ratio is increased but at a slower rate. The maximum peak pressure produced was 2200 kPa.

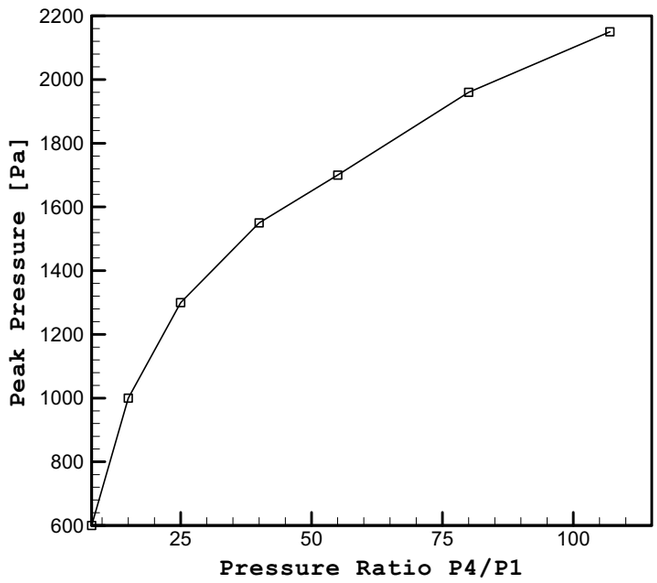

Fig. 41. Peak pressure vs. diaphragm pressure ratio P_4/P_1

5.4 The Effect of Gas Combination on the Facility Performance

Theoretical analysis showed that in order to achieve higher shock strength and shock speed, a gas combination with higher ratio of γ_4/γ_1 should be used. This can be achieved by using lighter gas in the driver section and heavier gas in the driven section. In the present work, combinations of He, CO_2 and Air were chosen. Other lighter gas such as Hydrogen was not used due to safety reason.

Figure 42 shows the pressure history at station (1) for pressure ratios of approximately 8, 15 and 20 respectively. The corresponding graphs at station (2) are plotted in Figures 43.

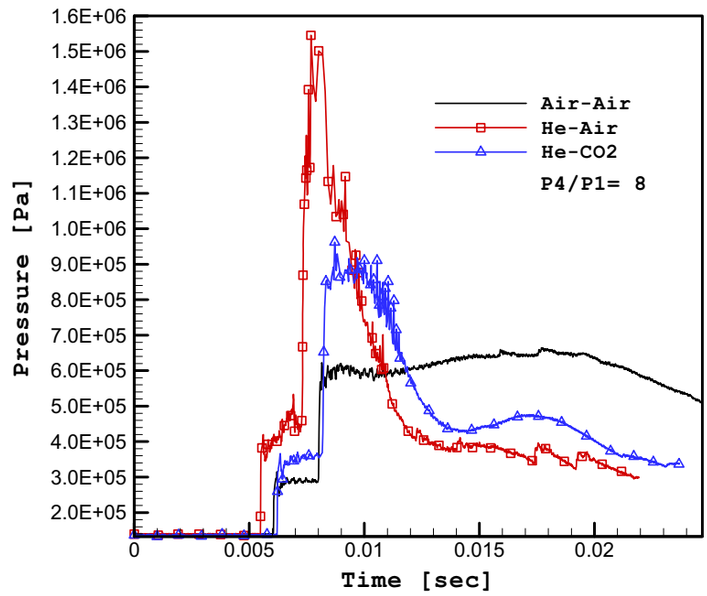

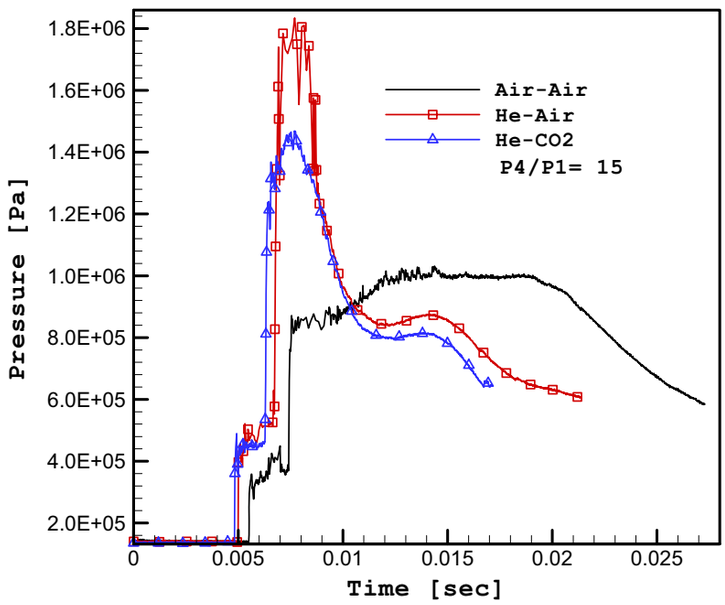

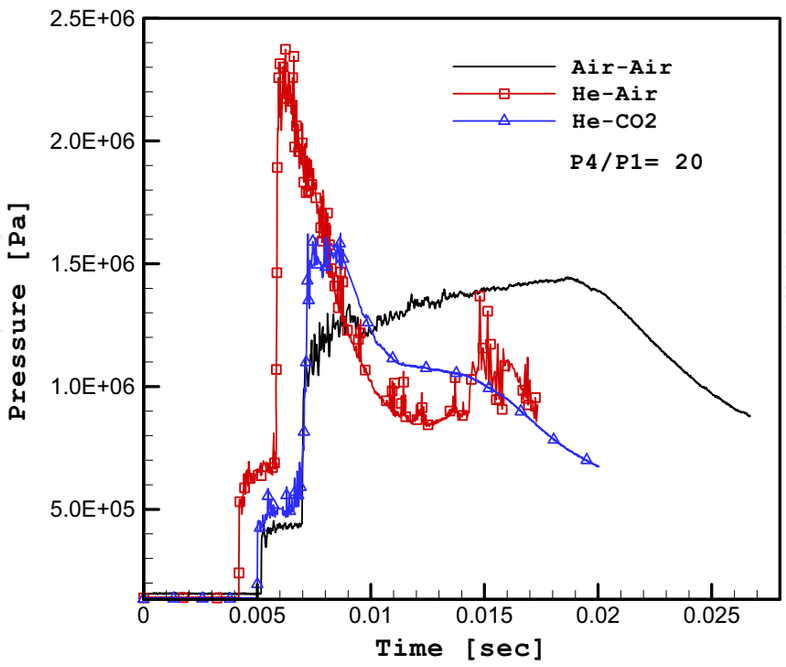

Fig. 42. Pressure history for three different gas combinations measured at station (1)

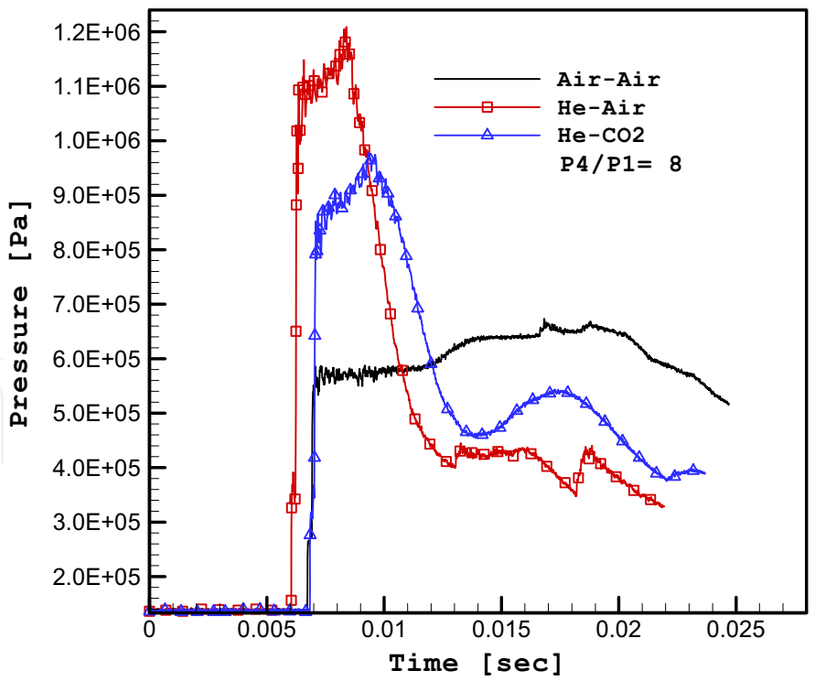

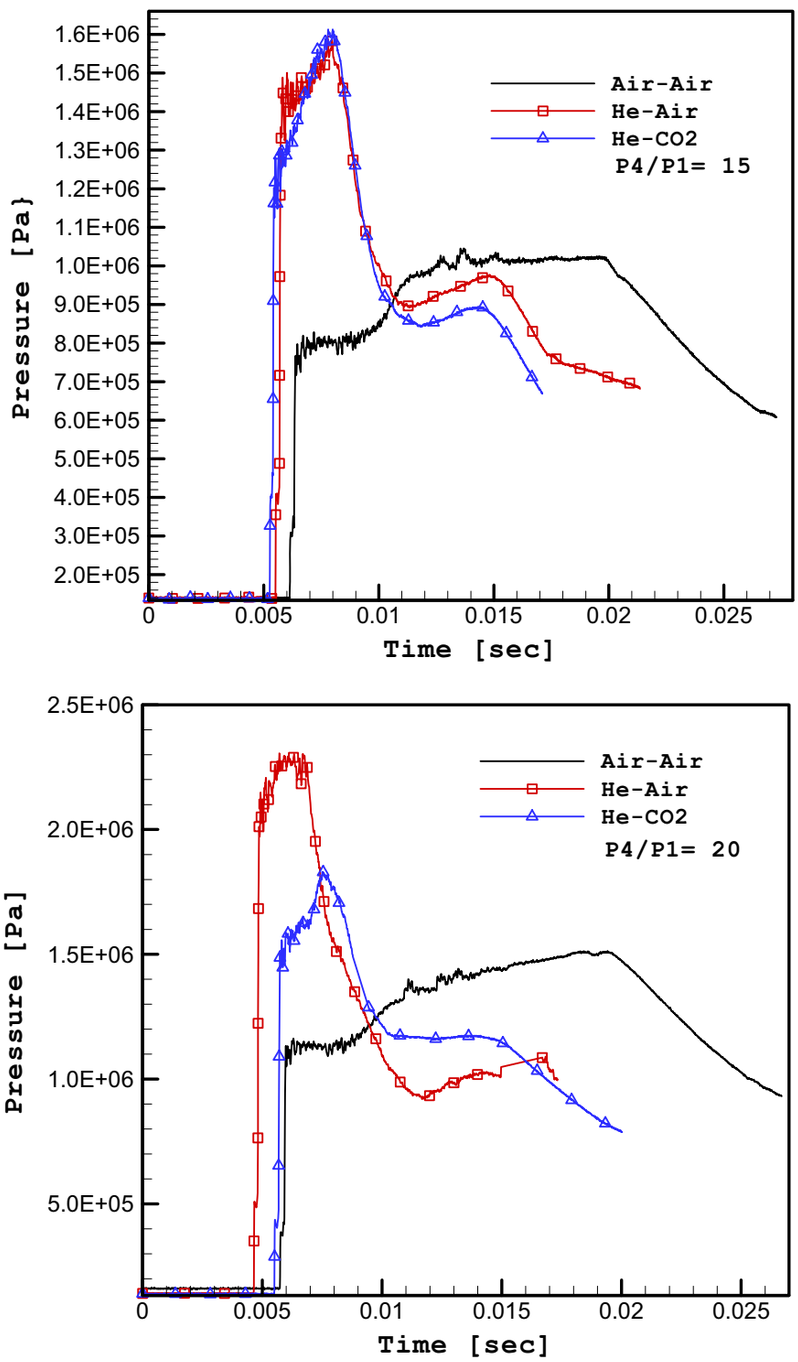

Fig. 43. Pressure history for three different gas combinations measured at station (2)

In general, it can be seen from Figures 42 and 43 that the He-Air gas combination provides the best results in terms of shock speed, shock strength and peak pressure. Comparing to Air-Air gas combination, He-CO_2 gives better shock strength and peak pressure. The

recorded initial rises at station (1) for He-Air are 400 kPa, 450 kPa and 650 kPa for 8, 15 and 20 pressure ratios respectively. After the shock reflection, the pressure rise further and peak pressure of 1500 kPa, 1800 kPa and 2400 kPa for pressure ratio 8, 15 and 20 respectively.
The experimental measurements were performed for pressure ratios from 8 to 55. Figures 44 and 45 show the measured shock speed and shock Mach number, respectively, for different gas combinations at various pressure ratios. Also plotted on the same graphs are the theoretical solutions.

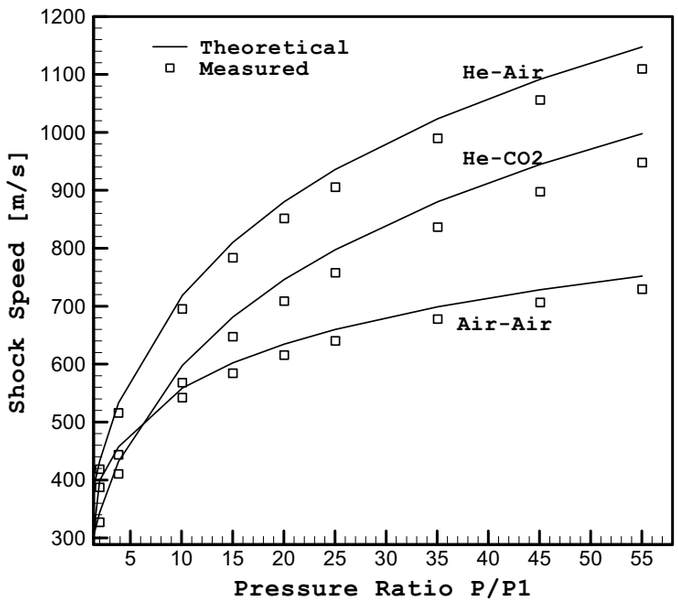

Fig. 44. Shock speed vs. pressure ratio for different gases

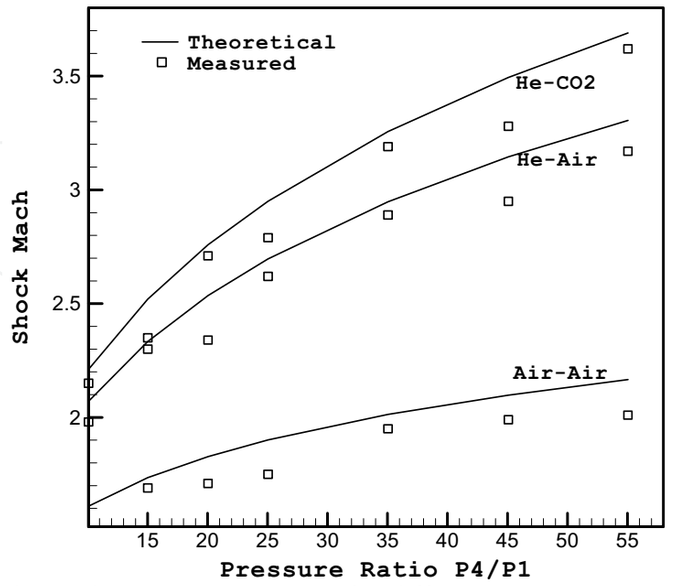

Fig. 45. Shock Mach number vs. pressure ratio for different gases

Similar to the Air-Air case, in general the measured data shows lower values compared to theoretical solution. However the trends are very similar. It can be seen that when γ_4/γ_1 is reduced the shock speed and Mach number increases. The maximum shock Mach number achieved was 3.69 when He-CO_2 was used at pressure ratio of 55. The peak pressure values achieved at various pressure ratios and gas combinations are plotted in Figure 46.

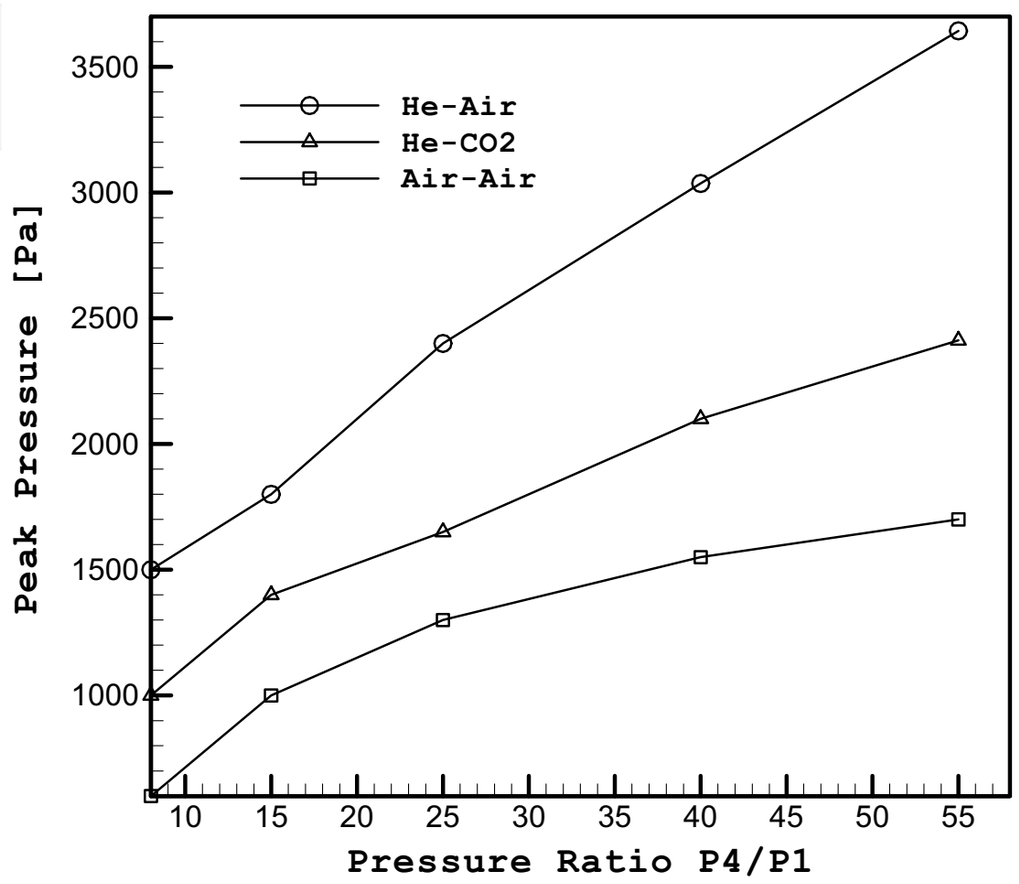

Fig. 46. Peak pressure vs pressure ratio P_4/P_1

5.5 The Effect of Piston on the Facility Performance

Previous researchers have shown that the addition of very light piston immediately after the diaphragm will increase the peak pressure achieved. After diaphragm rupture, the piston velocity will rapidly approach the contact surface velocity of a conventional shock tube. Multiple reflections of the shock wave ahead of the piston between the end of the driven section and the piston will compress the gas non-isentropically and result in a higher peak pressure.

Two experiments have been performed at pressure ratio P_4/P_1=13 for two gas combinations, Air-Air and He-Air. Figure 47 shows the pressure history at station (1) for Air-Air at pressure ratio P_4/P_1 = 13. The first pressure jump denoted by (1) is due to the shock wave passing as it moves from the piston to the end wall, whereas the second pressure rise

denoted by (2) is due to the reflected shock wave which causes further non-isentropic heating of the test gas. Between (1) and (2), the pressure gradually increases due to the compression by the piston. The shock wave will then be reflected from the piston and again moves towards the wall and cause the third pressure rise, denoted by (3). It will then reflect from the end wall and proceeds to the left causing further increase in pressure. The process of shock reflections and piston compressions are repeated a few more times causing further gas heating and pressure rise until the last one denoted by (5). Then there is a drop in pressure due to the fact that the piston has overshot its equilibrium position and has now been pushed to the left by compressed gas and come to rest. But the process of shock reflection continues to cause pressure rise, (6). This transient rapidly disappears as the pressure becomes equal on both sides of the piston.

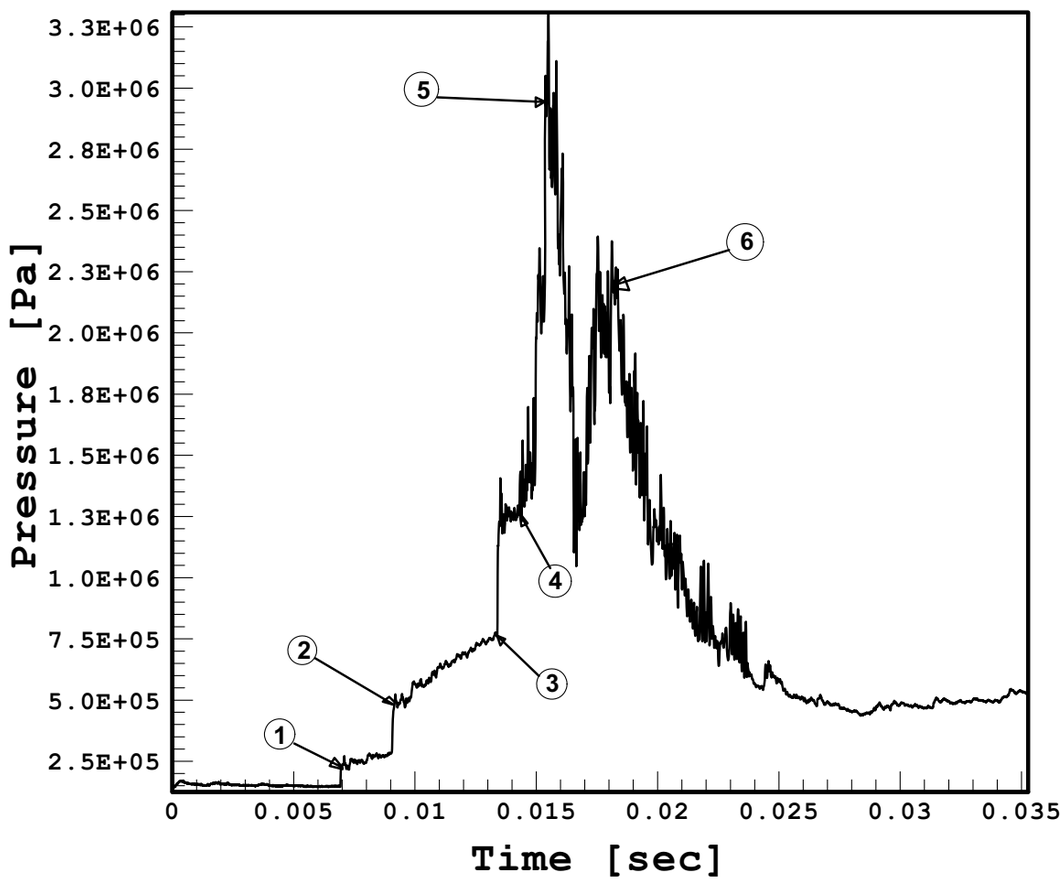

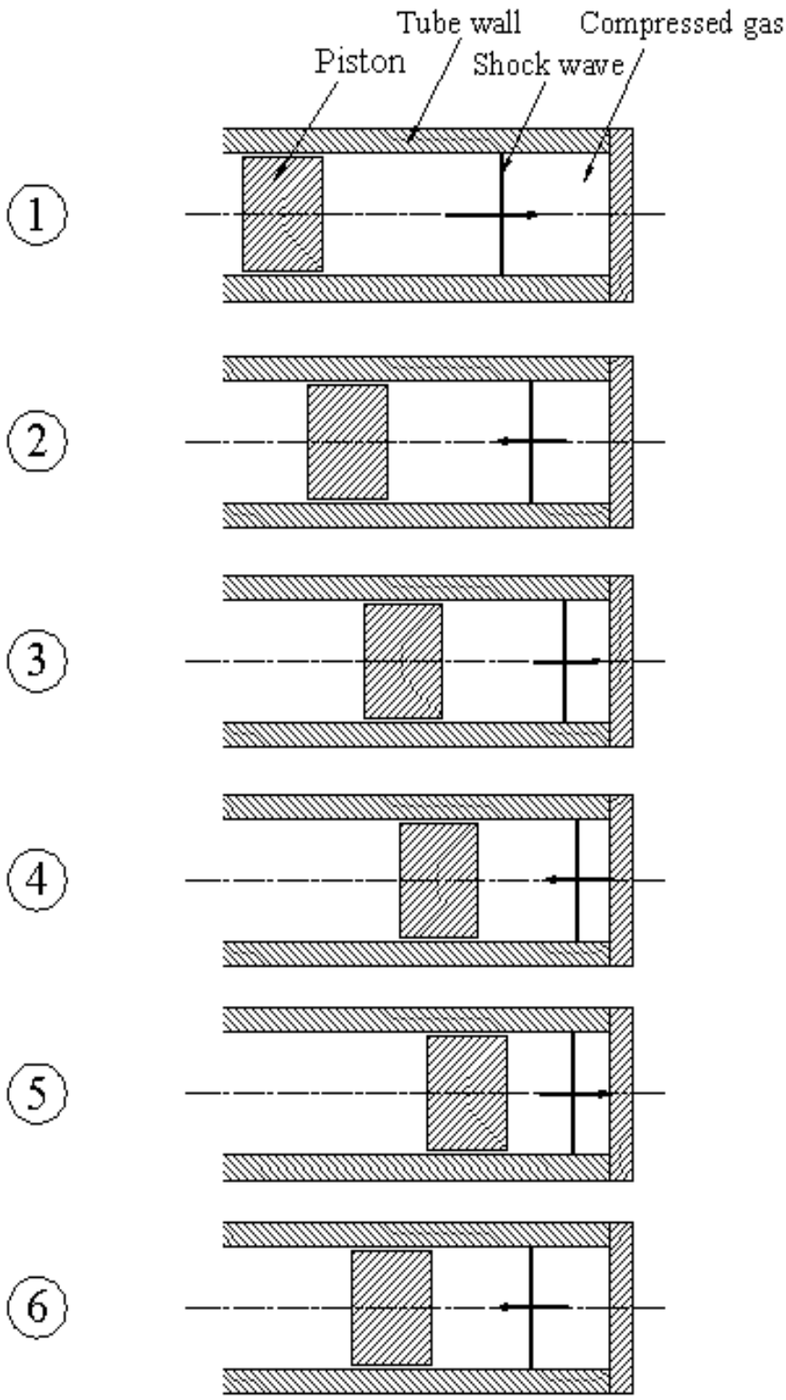

Fig. 47. Pressure history for free-piston compressor shot P_4/P_1=13 (Air-Air)

Figures 48 and 49 show the comparison of pressure transients at station (1) between cases with piston and without piston at pressure ratio 13 for Air-Air and He-Air gas combinations respectively.

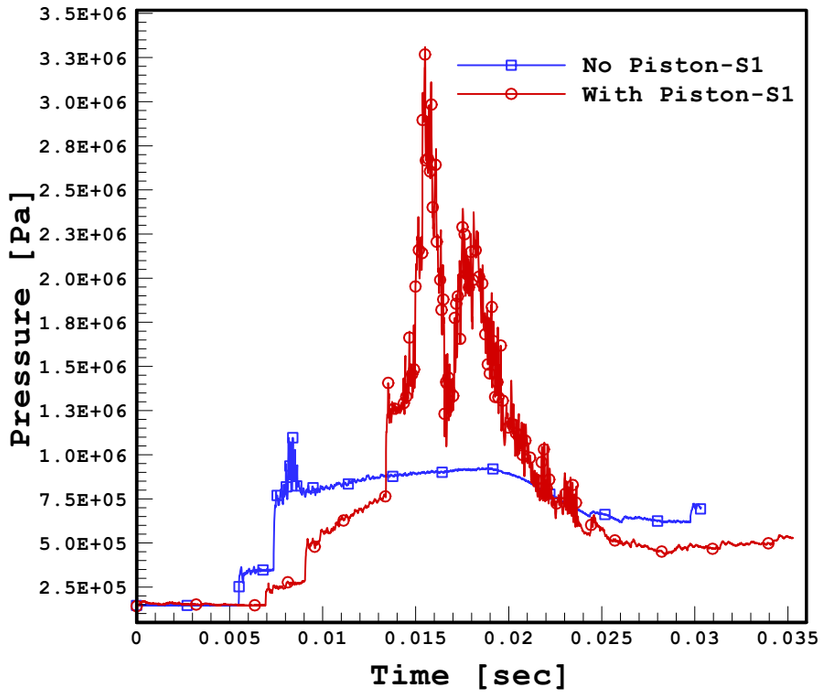

Fig. 48. Experimental pressure history inside driven section (Air-Air) P_4/P_1 =13

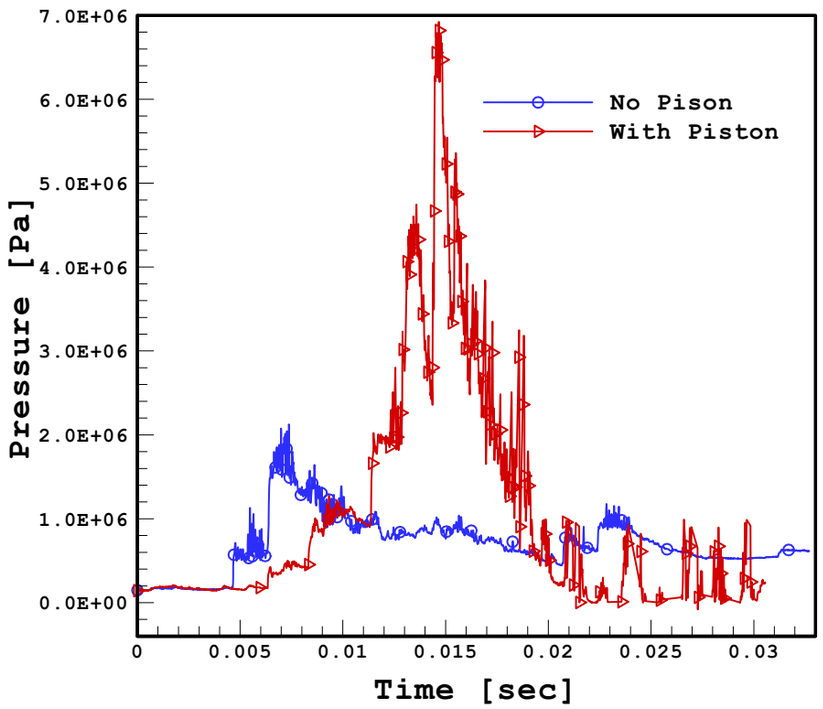

Fig. 49. Experimental pressure history inside driven section (He-Air) P_4/P_1 =13

It is apparent from Figures 48 and 49 that the shock speed is faster when the piston is not used, this is because the piston slows down the test gas ahead of it and consequently the shock will be slower. However, the peak pressure of that using piston is higher; the piston increases the peak pressure due to the compression process of the test gas. In spite of this, the He-Air as combination shows a tremendous improvement in terms of both shock strength and peak pressure. It is worth to mention here that the He-Air combination can produce a peak pressure of about 70 bar (with piston) as compared to that of Air-Air (33 bar), which has marked percentage of increase of more than 100%.
The shock speed and the shock Mach number can be obtained by comparing the pressure transient at station (1) and station (2). A sample result for Air-Air at pressure ratio 13 is shown in Figure 50. In this particular case the shock speed and shock Mach number is 441.3 m/s and 1.3 respectively.

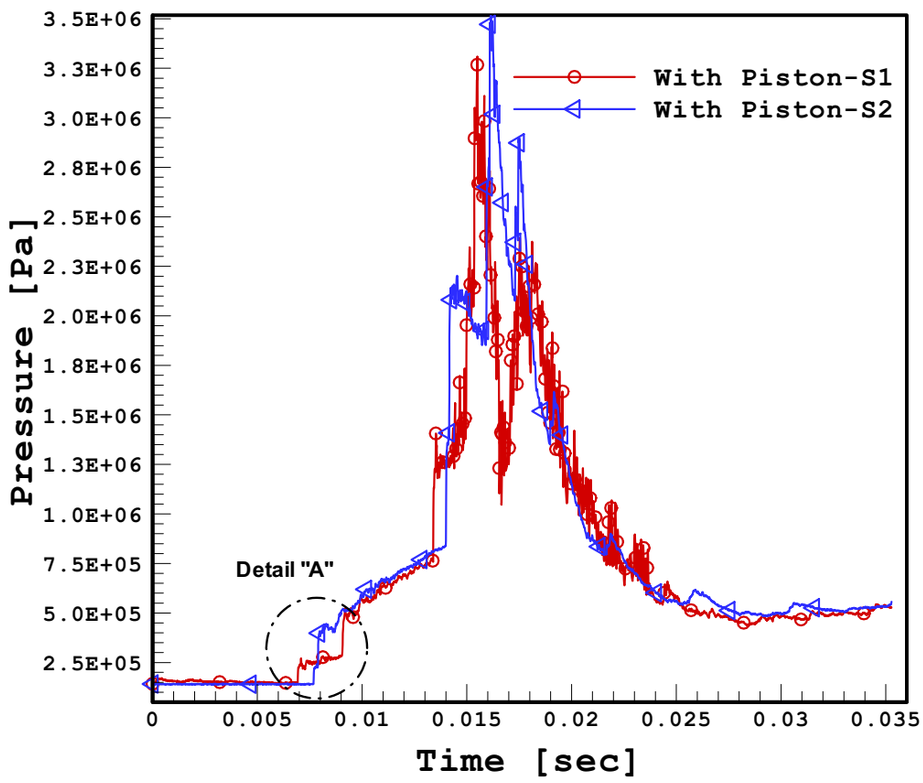

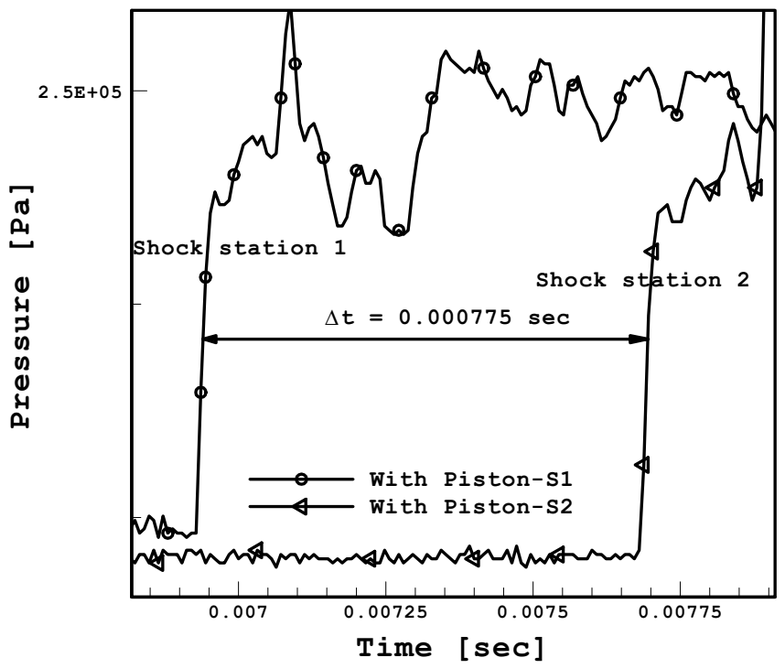

(a) Pressure history (b) Detail "A"

Fig. 50. Pressure history at station 1 and 2 (free piston compressor)

Similarly, Figure 51 shows the pressure history at stations 1 and 2 for shock tube shot.

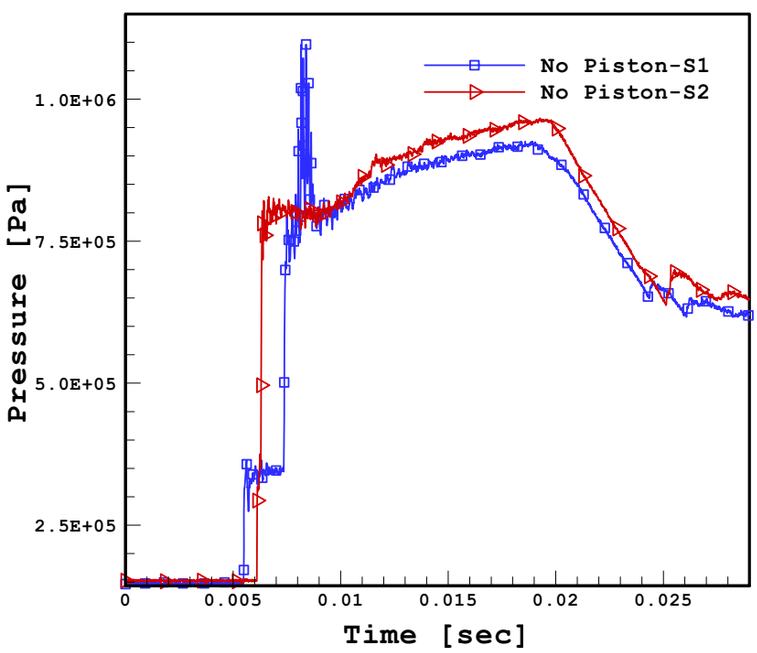

Fig. 51. Pressure history at station 1 and 2 (shock tube shot)

As explained previously, due to the piston effects in the free piston compressor test, the shock wave speed and shock Mach number for the shock tube shot are found to be higher, which are 570 m/s and 1.67 respectively.

5.6 Surface Temperature and Heat Flux

The gas temperature increase significantly during the test duration. For example, from the CFD results of Air-Air at a pressure ratio of 20 will produce gas temperature rise of 350 K. This high temperature rise, although for a very short duration will likely cause the tube wall temperature to rise and further cause heat loss that can affect the performance of the facility. In order to ascertain this effect, a surface junction thermocouple was used to measure the wall temperature during the test.

Figure 52 shows the surface temperature change measured experimentally at three different pressure ratio for shock tube shots with Air-Air gas combination. It clearly shows that the difference in surface temperature increases as the pressure ratio increases, which consequently enhance the undesirable heat loss to the surrounding. As explained previously, the first temperature jump is due to shock wave as it compresses the test gas and as the shock wave reflects from the end wall, further temperature rise is achieved.

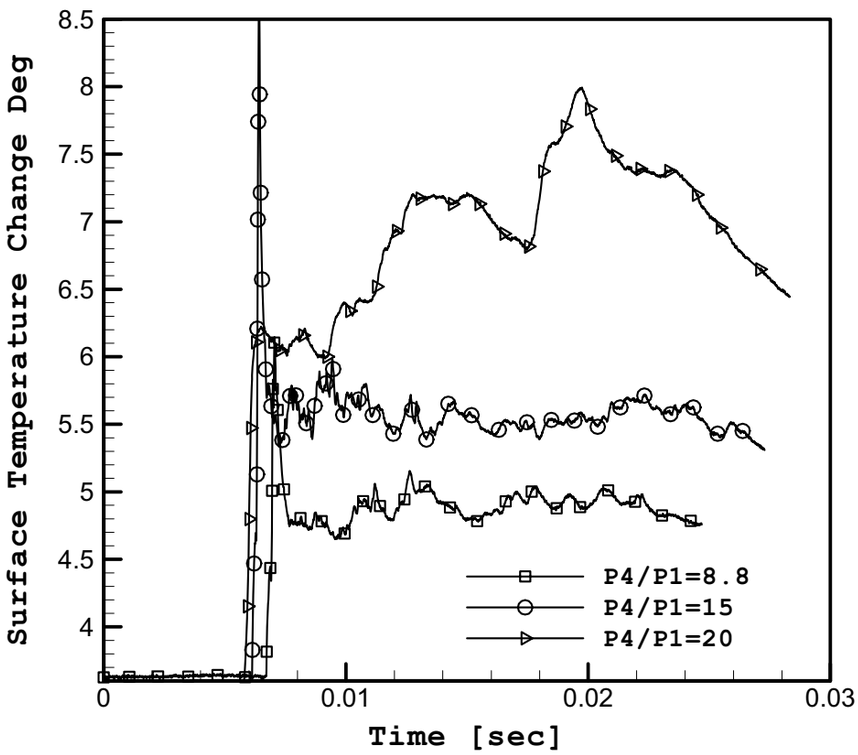

Fig. 52. Surface temperature change profile at different pressure ratios

The corresponding figure for the heat flux is shown in Figure 53 and as depicted, the heat flux increases after shock wave passes through the test gas, which may consequently, influence the facility performance.

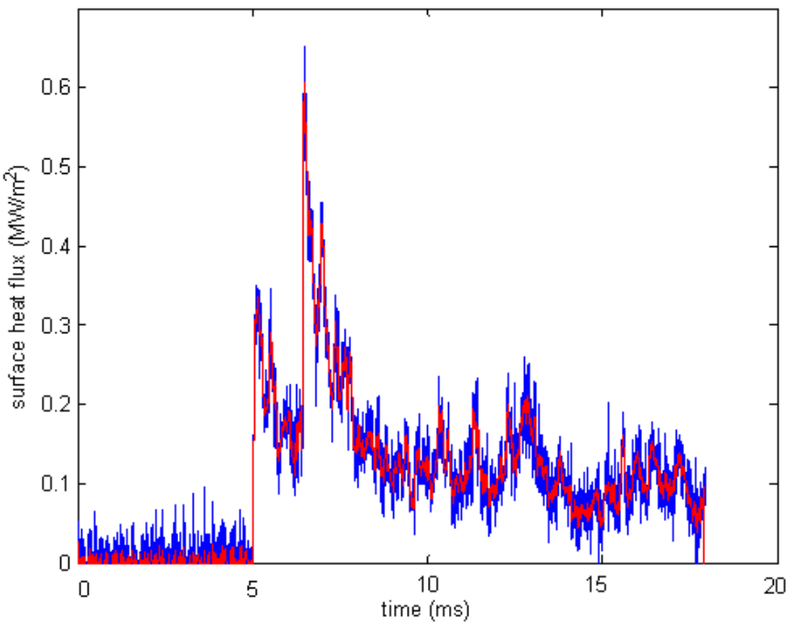

Fig. 53. Heat flux profile (shock tube shot)

Figure 54 presents surface temperature change for three gas combinations at a fixed pressure ratio of 8.4. The results show that maximum heat transfer occurs when He-Air was used.

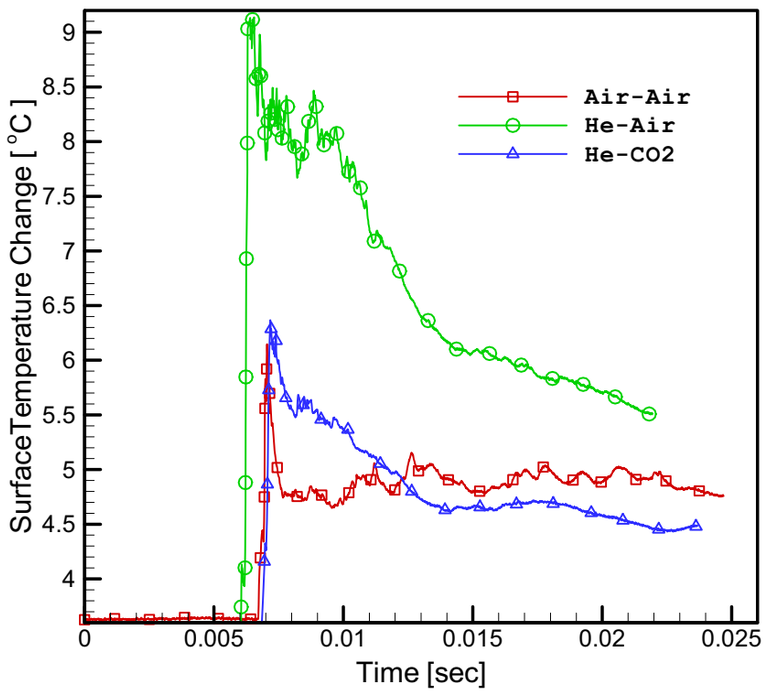

Fig. 54. Surface Temperature Change for different gas combinations at P_4/P_1= 8

The same trend can be observed for the free piston compressor shot as shown in Figure 55. It is worth mentioning here that the free piston compressor was able to produce a surface temperature change of about 4 °C (with piston) as compared to about 1.7 °C in the conventional shock tube indicating marked percentage increase of approximately 100%.

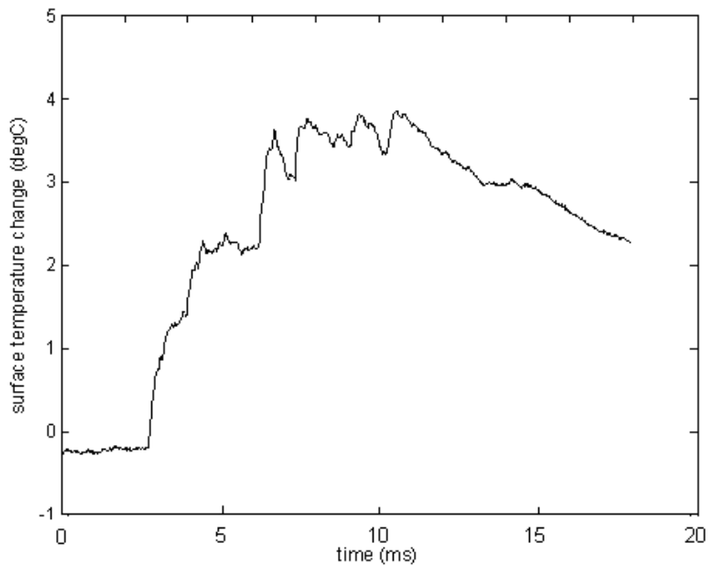

(a) Surface temperature change

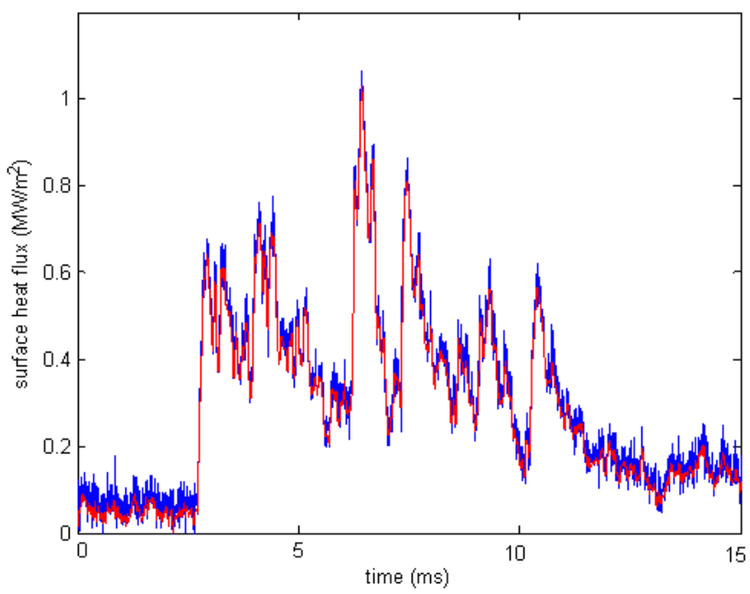

(b) Heat flux profile

Fig. 55. Surface temperature change and heat flux (free piston compressor shot)

6. Discussion and Conclusions

The goal of designing a high speed transient flow test facility with a relatively inexpensive price for research use has been achieved. This design for a multi arrangement high speed fluid flow tunnel will provide high speed fluid flows around test objects for actual flow measurement. Although the control of flow quality in such a tunnel would not be so easy, the actual ability for researchers to get their knowledge in real high speed fluid flow would be an immeasurable benefit.

The experimental and theoretical results agree very well with slight difference in shock speed values which are expected as the theoretical solution disregards the viscous, two dimensional and heat transfer effects which influence the shock strength and shock speed. It can be noted from results that time of shock wave creation for both experimental and CFD data are very much matched. The incident shock wave travels all the way along the driven section until it reflects off of the end wall. Similarly, the expansion wave reflects at the end of the driver section. The reflected shock then interacts with either the contact surface or the reflected expansion wave. It can be said that the general pattern of the experimental and CFD results are quite similar. Experiments showed that the shock wave speed for He/Air driver/driven gases is higher than He-CO_2 and Air/Air gas combinations for the same diaphragm pressure ratio.

Shock speed can be increased by raising the diaphragm pressure ratio, or more powerfully, by raising the speed of sound in the driver gas. To achieve high Mach numbers it is essential to raise the speed of sound ratio (a_4/a_1) if excessive pressures are to be avoided. Mach number of 3.69 is achieved and higher Mach number up to 6 is achievable by setting pressure ratio to P_4/P_1 = 465 using He-CO_2 or P_4/P_1 = 192 using H_2-CO_2. This ratio can be lowered by increasing temperature ratio T_4/T_1.

Results when employing different working fluids combination are also presented. The results showed a direct proportional relationship between Mach number and diaphragm pressure ratio and inverse proportion with speed of sound ratio.

The results show that for Air-Air driver/driven gases, the shock speed is decreased when piston is used. However, the peak pressure produced using piston is higher. The same trend can be observed for the He-Air combination. In spite of this, the latter shows a tremendous improvement in terms of both shock strength and peak pressure [17]. It is worth to mention, that He-Air combination can produce a peak pressure of about 70 bar for diaphragm pressure ratio P_4/P_1 equal to 13 only (with piston) as compared to that of Air-Air (33 bar) at the same diaphragm pressure ratio, which has marked a percentage of increase of more than 100%. This detailed information may be used to identify some of the causes for observed variations in pressure and temperature.

As the shock wave propagates in the driven section the test gas temperature rises up and consequently heat transfer to the tube wall causes an increase in the wall surface temperature. The same trend can be observed for the free piston compressor shot. It is worth to mention here that the free piston compressor can produce a surface temperature change of about 4 ^oC (with piston) as compared to that of conventional shock tube (1.7 ^oC), which has marked a percentage of increase of approximately 100%. The stagnation temperature achieved in free piston compressor is limited by the strength of the light piston used to compress the test gas, and the useful running time is restricted by the large heat losses to the cold walls of the tube.

The maximum testing time is varying between the arrival of the primary shock wave at the tube end, and the arrival of the first reflected wave, which has passed up the low pressure tube, reflected from the high pressure tube and returned to the nozzle station. The useful test time achieved from results was 10 ms which is quite comparable to other existing facilities.

Although this design showed good results, it should be noted that in the future, upgrades could be made to the facility to provide the better flow quality and longer flow times that would be needed for high speed fluid flow research. Detail design calculations, numerical simulations and experimental works have been conducted. The results presented in this chapter show that two-dimensional modeling of the high speed fluid flow test facility is an effective way to obtain facility performance data. Although this thesis focused on the UNITEN's facility, the CFD code is generic and may be applied to other facilities.

7. References

[1] Alan Pope and Kennith L. Goin, "*High-Speed Wind Tunnel Testing*", 2nd Edition, John Wiely", New York 1965.

[2] John D. Anderson, "*Modern Compressible Flow With Historical Perspective*", 2nd Edition, Mcgraw Hill, New York, 1990.

[3] Schultz and Jones 1973, "*A method for the accurate determination of the thermal product* $(\rho ck)^{1/2}$ *for thin film hat transfer or surface thermocouple gauges*" Phys. E: Sci Instrum. 21 445-448

[4] Morgan RG, Stalker, R. J. And Paull, A., "*Shock Tunnel studies of Scramjet Phenomena*", NASA contractor report 201694, 1997.

[5] East, R.A., "*The performance and operation of the University of Southampton hypersonic gun tunnel*", University of Southampton Aero. and Astro. Rep. no. 135, I960.

[6] Warren WR, Harris CJ, "*A critique of high performance shock tube driving techniques*" Shock Tubes Proc 7th Int Shock Tube Symp, June 23–25, 1969, ed. by I.I. Glass, University of Toronto Press, 143–176, 1970.

[7] Stalker RJ, "*A study of the free-piston shock tunnel*", AIAA J 5(12):2160–2165, 1967.

[8] Morgan RG, "*Development of X3, a superorbital expansion tube*", AIAA paper 2000-0558, 2000.

[9] Hannemann K, Beck WH, "*Aerothermodynamics research in the DLR high enthalpy shock tunnel HEG*", In: Lu FK, Marren DE (eds) Advanced hypersonic facilities. AIAA, Reston, Virginia, pp 205–237, 2002.

[10] Itoh K, "*Characteristics of the HIEST and its applicability for hypersonic aerothermodynamic and scramjet research*", In: Lu FK, Marren DE (eds) Advanced hypersonic facilities. AIAA, Reston, Virginia, pp 239–253, 2002.

[11] Al-Falahi Amir 'Design, Consruction and Performance Evaluation of a Short Duration High Speed Flow Test Facility' Ph.D. Thesis, Universiti Tenaga Nasional, 2008.

[12] Al-Falahi Amir, Yusoff M. Z & Yusaf T "*Numerical Simulation of Inviscid Transient Flows in Shock Tube and its Validations*" proceedings of world academy of science, engineering and technology volume 33, Heidelberg, Germany, September 24-26, 2008 issn 2070-3740

[13] Drazin, P.G. and Reid, W.H. "*Hydrodynamic Stability"*, Cambridge Monographs on Mechanics and Applied Mathematics, Cambridge University Press 1993.

[14] Al-Falahi Amir, Yusoff M. Z & N. H. Shuaib "Flow Instability in Shock Tube Due to Shock Wave-Boundary Layer-Contact Surface Interactions, a Numerical study" European Journal of Scientific Research, accepted March 2009.

[15] Xu Fu and Xu Cuiwei, "*Instability theory of shock wave in a shock tube*", Journal of Acta Mechanica Sinica, ISSN 0567-7718 (print) 1614-3116 (Online), Volume 8, Number 2/May, Springer Berlin /Heidelberg,1992.

[16] McKenzie, Nick R., "*The effect of viscous attenuation on shock tube performance*", M.S. Thesis Air Force Inst. Of Tech., Wright-Patterson AFB, OH., 1994.

[17] Al-Falahi Amir, Yusoff M. Z & Yusaf T "*An Experimental Evaluation of Shock Wave Strength and Peak Pressure in a Conventional Shock Tube and Free-Piston Compressor*", Proceedings of IMECE2008, 2008 ASME International Mechanical Engineering Congress and Exposition November 2-6, 2008, Boston, Massachusetts, USA

New Trends in Technologies

Edited by Blandna ramov

ISBN 978-953-7619-62-6

Hard cover, 242 pages

Publisher InTech

Published online 01, January, 2010

Published in print edition January, 2010

This book provides an overview of subjects in various fields of life. Authors solve current topics that present high methodical level. This book consists of 13 chapters and collects original and innovative research studies.

How to reference

In order to correctly reference this scholarly work, feel free to copy and paste the following:

Al-Falahi Amir, Yusoff M. Z, N. H. Shuaib and Yusaf T (2010). A Comprehensive Performance Evaluation of a Short Duration High Speed Transient Flow Test Facility, New Trends in Technologies, Blandna ramov (Ed.), ISBN: 978-953-7619-62-6, InTech, Available from: http://www.intechopen.com/books/new-trends-in-technologies/a-comprehensive-performance-evaluation-of-a-short-duration-high-speed-transient-flow-test-facility

INTECH
open science | open minds

InTech Europe
University Campus STeP Ri
Slavka Krautzeka 83/A
51000 Rijeka, Croatia
Phone: +385 (51) 770 447
Fax: +385 (51) 686 166
www.intechopen.com

InTech China
Unit 405, Office Block, Hotel Equatorial Shanghai
No.65, Yan An Road (West), Shanghai, 200040, China
中国上海市延安西路65号上海国际贵都大饭店办公楼405单元
Phone: +86-21-62489820
Fax: +86-21-62489821

IntechOpen